



Review

# Carbon Nanostructures Doped with Transition Metals for Pollutant Gas Adsorption Systems

J. M. Ramirez-de-Arellano <sup>1</sup>, M. Canales <sup>2</sup> and L. F. Magaña <sup>3,\*</sup>

<sup>1</sup> Escuela de Ingeniería y Ciencias, Tecnológico de Monterrey, Av. Eugenio Garza Sada 2501, Monterrey 64849, Mexico; jramirezdearellano@tec.mx

<sup>2</sup> Universidad Autónoma Metropolitana Unidad Azcapotzalco, Av. San Pablo Xalpa No. 180, Colonia Reynosa Tamaulipas, Delegación Azcapotzalco, Ciudad de México 02200, Mexico; monic.canales@gmail.com

<sup>3</sup> Instituto de Física, Universidad Nacional Autónoma de México, Apartado Postal 20-364, Ciudad de México 01000, Mexico

\* Correspondence: fernando@fisica.unam.mx

**Abstract:** The adsorption of molecules usually increases capacity and/or strength with the doping of surfaces with transition metals; furthermore, carbon nanostructures, i.e., graphene, carbon nanotubes, fullerenes, graphdiyne, etc., have a large specific area for gas adsorption. This review focuses on the reports (experimental or theoretical) of systems using these structures decorated with transition metals for mainly pollutant molecules' adsorption. Furthermore, we aim to present the expanding application of nanomaterials on environmental problems, mainly over the last 10 years. We found a wide range of pollutant molecules investigated for adsorption in carbon nanostructures, including greenhouse gases, anticancer drugs, and chemical warfare agents, among many more.

**Keywords:** carbon nanostructures; doping; adsorption; transition metals; pollutant gas; nanotubes; graphene; fullerenes; graphdiyne; buckybowls



**Citation:** Ramirez-de-Arellano, J.M.; Canales, M.; Magaña, L.F. Carbon Nanostructures Doped with Transition Metals for Pollutant Gas Adsorption Systems. *Molecules* **2021**, *26*, 5346. <https://doi.org/10.3390/molecules26175346>

Academic Editor: Teobald Kupka

Received: 28 July 2021

Accepted: 31 August 2021

Published: 2 September 2021

**Publisher's Note:** MDPI stays neutral with regard to jurisdictional claims in published maps and institutional affiliations.



**Copyright:** © 2021 by the authors. Licensee MDPI, Basel, Switzerland. This article is an open access article distributed under the terms and conditions of the Creative Commons Attribution (CC BY) license (<https://creativecommons.org/licenses/by/4.0/>).

## 1. Introduction

Since their discovery in 1985, the study of fullerenes and their exciting properties led to the subsequent discovery of many other carbon nanoforms: nanotubes, carbon onions, graphene, graphdiyne, carbon nanotori, etc., including hybrid nanostructures [1–6], see Figures 1 and 2. As a result, there are numerous practical applications of carbon nanostructures, like gas sensors, adsorption of pollutant molecules, electric batteries, hydrogen adsorption, electronic devices, etc.

The capture of gases like CO, CO<sub>2</sub>, N<sub>2</sub>O, CH<sub>4</sub>, and many others is urgent. CO comes mainly from the non-complete combustion of fuels that contain carbon, and it is toxic and an asphyxiant. On the other hand, plenty of industrial processes in our world generate greenhouse gases like CO<sub>2</sub>, N<sub>2</sub>O, and CH<sub>4</sub>. Thus, humankind's climate change and ecological challenges have increased the interest in carbon nanostructures for fast green applications [7].

We should mention that the specific surface area of graphene is 2630 m<sup>2</sup>/g, more significant than that of zeolites (between 500 and 800 m<sup>2</sup>/g) although smaller than that of metal-organic frameworks (or MOFs), which is around 7000 m<sup>2</sup>/g.

Thus, carbon nanostructures' sizeable specific surface area is an excellent appeal for gas sensing and gas adsorption systems. Furthermore, the adequate doping of these structures may increase their adsorption capability and tune their selective adsorption. In particular, the reactivity of transition metals makes them ideal dopant candidates. Investigations based on the density functional theory (DFT) have been crucial to explore the adsorption properties of the different carbon nanostructures. Some researchers studied the variability in results obtained from diverse DFT implementations. For instance, predictions

made using the Augmented Plane Waves plus local orbitals method (APW+lo) and the Projector Augmented Wave method (PAW) are identical for practical purposes [8]. Most of the computational studies reviewed in this paper also report the density of states (DOS) spectrum to complement their investigations on carbon nanostructures. They also include Mulliken or Lowdin charge analysis, electron density differences, HOMO and LUMO analysis, etc. In general, DFT is very efficient in computing interaction energies, while the Grand Canonical Monte Carlo (GCMC) calculations are adequate to predict adsorption capacities.

This work aims to review the most important and recent developments related to the adsorption of pollutants or hazardous gases by using carbon nanostructures. Among the most investigated pollutant gases, we must mention carbon monoxide (CO), carbon dioxide (CO<sub>2</sub>), methanol (CH<sub>3</sub>OH), methane (CH<sub>4</sub>), nitrogen monoxide (NO), nitrogen dioxide (NO<sub>2</sub>), ozone (O<sub>3</sub>), and formaldehyde (CH<sub>2</sub>O) with many others. However, we found some works on hydrogen adsorption on carbon nanostructures, which is essential to serve as a non-pollutant fuel. Although, we should mention that the number of works on this subject in the last 10 years is considerably less than previously.

We covered a 10-year range approximately, not in an exhaustive way, but describing the state-of-the-art up to date. When results were considered relevant enough, or when we believed that they would add important information for the context of the topic covered, we also included works dating from earlier years.

In the second section, we review the adsorption of molecules on undoped or non-metal functionalized carbon nanostructures. We considered the subsections of nanotubes, graphene, fullerenes, graphdiyne, and hybrid systems. The third section reviews the same carbon structures as in the second section but doped with transition metals. Our conclusions are in the fourth section.

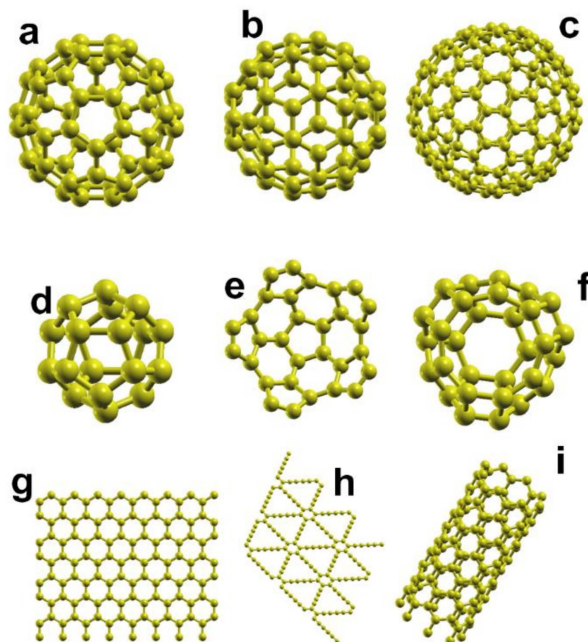


**Figure 1.** These are some of the carbon nanostructures reported experimentally. In (a,b), we have C<sub>60</sub>; we present the C<sub>180</sub> in (c); C<sub>20</sub> in (d); the buckybowl C<sub>30</sub> in (e,f); graphene in (g); graphdiyne in (h); a single-walled carbon nanotube (SWCNT) in (i).

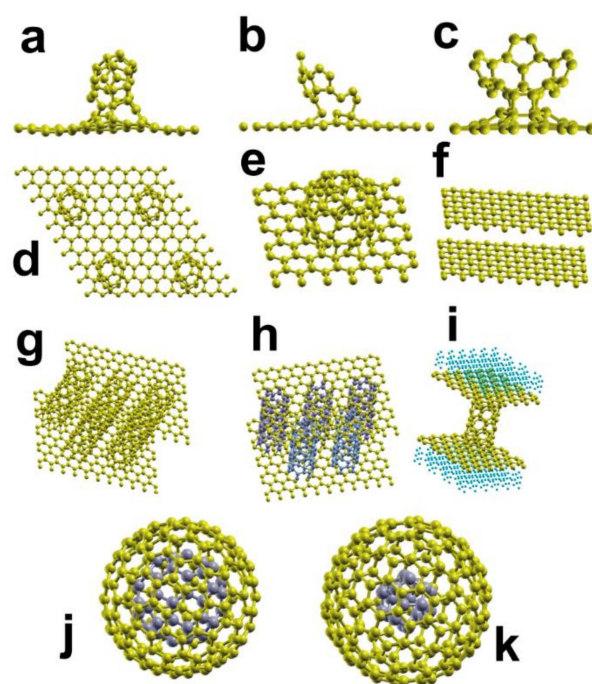


**Figure 2.** We present some of the hybrid carbon nanostructures reported experimentally. In (a–d), we have a C<sub>30</sub> (a buckybowl) adsorbed on graphene; in (e), we show a fullerene C<sub>60</sub>, adsorbed on graphene; we show in (f), a bi-layer graphene; in (g,h), we present pillared graphene with nanotubes (SWCNTs); in (i) we show pillared graphene with hydrogen; we present in (j,k), two examples of carbon nano onions (CNO).

## 2. Adsorption of Molecules on Pristine or Nonmetal Functionalized Systems

### 2.1. Nanotubes

Various experimental studies focus on the gas adsorption capabilities of single-walled carbon nanotubes (SWCNTs) and multiple walled carbon nanotubes (MWCNTs), showing a good agreement with the Langmuir adsorption model. The nature of the gas sensing mechanism in nanotubes would be due to charge transfer between them and the molecules adsorbed, or due to effects of the carbon nanotube network, for devices made of bundles [9].

Several works using first-principles calculations have also shed light on this topic. Numerical DFT simulations using the local density approximation (LDA) for the exchange-correlation potential show that most gas molecules adsorb weakly on pristine SWCNTs. Still, certain gases like NO<sub>2</sub> and O<sub>2</sub> are more sensitive to be adsorbed due to the electronic properties of the former [10]. Although LDA is usually inaccurate to describe long-range interactions, the molecule-tube interaction seems to be between the LDA and the generalized gradient approximation (GGA). Hydrogen adsorption is another broad field of interest due to its potential applications as a non-pollutant fuel. Experimental studies suggest that fold-structure adsorbents convey better H<sub>2</sub> adsorption than pore or flat structures [11]. It is common to characterize the carbon material by N<sub>2</sub> adsorption at a given temperature and correlate that to their hydrogen storage capacity. SWNTs perform below activated carbon samples for hydrogen uptake, but the process is reversible in both cases. The storage capacity of the latter is about 4.5 wt% at 77 K [12]. Functionalizing MWCNTs using acids (F-MWCNTs) or by KOH activation (A-MWCNTs) increases the H<sub>2</sub> gas sensing response [13,14].

The adsorption uptake of CO<sub>2</sub> in pristine SWCNTs is more significant than that of CO, CH<sub>4</sub>, N<sub>2</sub>, and H<sub>2</sub>, a result that is confirmed both experimentally and by Monte Carlo simulations [15]. Experimental results show that carbon nanotubes, when modified by 3-aminopropyl-triethoxysilane (APTS), adsorb CO<sub>2</sub> better. This effect decreases with temperature and increases with water content in the air. MWCNTs modified by APTS

have good adsorption performance at 20 °C. The interaction between molecules and CNTs-APTS implies physisorption and chemisorption that shows stability for a cyclic operation. This operation is enhanced using saturated water vapor in the gas stream, giving CO<sub>2</sub> deconcentration of around 67% [16–18]. Carbon nanotubes films have also been studied as CO<sub>2</sub> sensors, both experimentally and via grand canonical Monte Carlo (GCMC) simulations [19].

Some other ways of increasing the adsorption capacity of CO<sub>2</sub> are by functionalizing carbon nanotubes with nitrogen groups (N-MWCNTs); by fabricating polyethylenimine-polyethylene glycol/MWCNTs bilayer-structure devices—obtaining CO<sub>2</sub> desorption without heating; or by a two-step modification of MWNTs using a mixture of diluted nitric and sulfuric acid and then 1,3-diamino propane [20–22].

The diameter and chirality of CNTs affect the adsorption. Flexible SWCNTs would adsorb up to 35 wt% of CO<sub>2</sub>, as studied using molecular dynamics (MD) calculations, including ad hoc potentials built to model the intramolecular interactions within the SWCNT [23].

The selectivity of CO<sub>2</sub>/CH<sub>4</sub>—i.e., good adsorption of CO<sub>2</sub> combined with the exclusion of CH<sub>4</sub>—also increases by this functionalization, an effect that reaches an optimal value at lower pressures and room temperature, which is essential for industrial gas separation. Oxygen-rich surface functional groups attached to the surface of MWCNTs also increase the CO<sub>2</sub> adsorption capacity [20,24]. MWCNTs physisorb methane (CH<sub>4</sub>) and natural gas showing fast sorption kinetics, making MWCNTs a promising porous media for natural gas storage [25]. Applying high pressures to double-walled carbon nanotube arrays increases the CO<sub>2</sub> and N<sub>2</sub> gas adsorption, an effect that is also obtained by functionalizing the tubes via oxygen plasma treatment [26]. GCMC simulations also indicate that water molecules can increase the selectivity of CO<sub>2</sub> when CO<sub>2</sub>/CH<sub>4</sub> and H<sub>2</sub>O/CO<sub>2</sub>/CH<sub>4</sub> mixtures are considered in CNTs and silicon carbide-derived carbon (SiC-DC) [27].

Sulfur hexafluoride (SF<sub>6</sub>) is another greenhouse gas, considered several orders of magnitude more nocive than CO<sub>2</sub>, measured over long periods. MWNTs modified via H<sub>2</sub>SO<sub>4</sub>/H<sub>2</sub>O<sub>2</sub> oxidation, or KOH activation, are suitable SF<sub>6</sub> adsorbents [28].

The adsorption of acetone (C<sub>3</sub>H<sub>6</sub>O) is another issue extensively studied. This substance is liquid at room temperature, and it has a low boiling point of 329.20 K or 56.05 °C [29]. SWCNTs can strongly adsorb acetone molecules and then desorb them with increasing temperature within the interval of 400–900 K. For large-diameter SWCNTs, adsorption can happen in the interstitial channels, the bundles. The elastic deformation of the tubes can also increase the adsorption of acetone molecules [30]. Similar studies have been performed combining experimental and DFT methods to study the ethanol (C<sub>2</sub>H<sub>5</sub>OH) sensing properties of CNTs [31]. Polyaniline functionalized multiwalled carbon nanotubes (PANI/MWCNTs) have also been experimentally shown to detect ammonia (NH<sub>3</sub>) gas [32].

There are other ways of increasing the sensing performance of CNTs, besides deformation. For instance, sorted semiconducting nanotubes are more sensitive to pollutant gases like NO<sub>2</sub> and NH<sub>3</sub> than unsorted tubes [33]. For nitric oxide (NO) adsorption, in situ ultraviolet (UV) light illumination of pristine carbon nanotubes can increase their performance. The cleaning of the surface of the tubes by UV light would improve their gas sensing capacity [34]. Chemical polymerization with pyrrole (PPy) to obtain SWNTs/PPy nanocomposites can also enhance their sensitivity 10 times [35].

We found investigations of recent years on the adsorption of other gas molecules, like Xe, natural gas, or the nitrate ion NO<sub>3</sub>. The adsorption of Xe by single-walled carbon nanotubes (SWCNTs) has been studied experimentally and using ab initio calculations. Closed SWCNTs can be opened by oxidation at their ends and wall defect sites using ozone. This opening enhances the adsorption of Xe, as the nanotube etching increases wall openings at an optimal radius of 5–7 Å. After these optimal values, the adsorption rate drops [36]. SWCNTs can also adsorb a nitrate ion NO<sub>3</sub><sup>−</sup> in its gas phase [37].

Carbon nanotubes can also adsorb formaldehyde (HCHO) molecules in their interior and exterior walls, with preferential adsorption on the latter. The adsorbed HCHO

molecules alter the electronic structure of the CNNTs, reducing the HOMO/LUMO gap from its original value of 4.02 to 2.44 eV, according to ab initio calculations [38]. These tubes can adsorb mixtures of SO<sub>2</sub>/N<sub>2</sub> at the equimolar ratio, with MD calculations showing an increase in SO<sub>2</sub> adsorption as the CNT diameter increases [39]. Finally, experimental studies have demonstrated the feasibility of MWCNTs as adsorbents of several volatile organic compounds (VOCs) such as benzene, methanol, ethanol, acetone, etc. [40].

Table 1 summarizes the adsorption energies—for the studies that reported them—and the characteristics of investigations covered in this section. When the study considers different variations or adsorption conditions for the same adsorbate, an energy range is given instead of a particular value.

**Table 1.** Summary of adsorption energies  $E_{\text{ads}}$  (in eV) for different non-metallic doped nanotubes systems and adsorbates. The type of study is also specified.

System	Type of Study	Adsorbate	$E_{\text{ads}}$
CNTs [41]	DFT	NO <sub>2</sub>	−0.427
		CH <sub>4</sub>	−0.122
		CO <sub>2</sub>	−0.109
SWCNTs [39]	GCMC, MD	SO <sub>2</sub>	−0.464
MWCNTs [11]	Experimental	H <sub>2</sub>	[−0.26, −0.046]
MWNTs [28]	Experimental	SF <sub>6</sub>	[−0.529, −1.285]
SWCNTs [37]	DFT	NO <sub>3</sub>	−1.30
CNNT [38]	DFT	H <sub>2</sub> CO	−0.321
		NO <sub>2</sub>	−0.427
		O <sub>2</sub>	−0.306
		H <sub>2</sub> O	−0.128
		NH <sub>3</sub>	−0.162
		N <sub>2</sub>	−0.123
		CO <sub>2</sub>	−0.109
		CH <sub>4</sub>	−0.122
		Ar	−0.082
		H <sub>2</sub>	−0.056
SWCNTs [12]	Experimental	CO <sub>2</sub>	−0.005
SWCNTs and SiC-DC [27]	GCMC	CH <sub>4</sub>	−0.003
		C <sub>3</sub> H <sub>6</sub> O	[−0.255, −0.771]
		C <sub>2</sub> H <sub>5</sub> OH	Not reported
SWCNTs [30]	Exp. and DFT	CO <sub>2</sub>	Not reported
CNTs [31]	Experimental	VOC	Not reported
CNTs films [19]	Exp. and GCMC		
MWCNTs [40]	Experimental		
SWCNTs [36]	Exp., GCMC, MD	Xe	Not reported
F-MWCNTs [24]	Experimental	CO <sub>2</sub>	[−0.084, −0.036]
F-MWCNTs [13]	Experimental	H <sub>2</sub>	Not reported
Oxygen F-CNTs [26]	Experimental	C <sub>2</sub> , N <sub>2</sub>	Not reported
PANI/MWCNTs [32]	Experimental	NH <sub>3</sub>	Not reported
F-MWCNTs and A-MWCNTs [14]	Experimental	H <sub>2</sub>	Not reported
1,3-diaminopropane MWCNTs [22]	Experimental	CO <sub>2</sub>	Not reported

## 2.2. Graphene

Typical calculations of molecules adsorption on graphene consider either a 4 × 4 or a 5 × 5 unit cell to avoid spurious interactions, as many codes work with periodic boundary conditions. The three adsorption sites considered in these studies are (a) at the bond between two C atoms or a B-site; (b) at the top of a C atom or T-site; (c) over the center of a hollow hexagon of C atoms, or H-site. Most DFT calculations work with a graphene monolayer, but some studies consider two or more sheets.

The adsorption of atomic or molecular hydrogen on graphene has attracted much interest in the last decade. Graphene can adsorb H atoms with binding energies per atom of about 0.8–1.9 eV [42]. There are predictions of theoretical calculations that hydrogenated graphene sheet would be a semiconductor. Deuterium (D) has been incorporated

into graphene via thermal annealing in a process above 400 °C, which is not entirely reversible [43] to verify those predictions. Defects in graphene can also improve H<sub>2</sub> adsorption. Defective graphene V<sub>222</sub> is obtained by removing a C atom from the graphene sheet and then di-hydrogenating the three C atoms on the vacancy edges. MD calculations using a V<sub>222</sub> structure show an H<sub>2</sub> adsorption–desorption process that is more reversible than pristine graphene [44].

It is frequent to find graphene used as a substrate to adsorb H<sub>2</sub>O, NH<sub>3</sub>, CO, NO<sub>2</sub>, and NO, as explored via DFT ab initio calculations and experimentally. It is well established that pristine graphene adsorbs H<sub>2</sub>O molecules, with the latter acting as an acceptor. NO<sub>2</sub> can also be physisorbed on pristine graphene, and it can induce more significant doping than NO [45,46]. Pristine graphene can physisorb NO molecules with electrons transferred from the first to the second, with the B-site being the most stable adsorption site [47]. It can also weakly adsorb hydrogen sulfide (H<sub>2</sub>S) and methane (CH<sub>4</sub>) [48]. NonTM-functionalized graphene can also detect ammonia (NH<sub>3</sub>). A way to increase the sensing performance of graphene is to produce pristine graphene noncovalently functionalized, usually by a biocompatible stabilizer such as flavin mononucleotide sodium salt [49].

From experimental and theoretical investigations, we find that graphene can adsorb organic molecules such as acetone, acetonitrile, dichloromethane, ethanol, ethyl acetate, hexane, and toluene. Graphene modeled as coronene would interact with said molecules primarily by London dispersive forces [50]. Table 2 summarizes the main results reviewed in this section.

**Table 2.** Summary of adsorption energies E<sub>ads</sub> (in eV) for different non-metallic doped graphene systems and adsorbates. The type of study is also specified.

System	Type of Study	Adsorbate	E <sub>ads</sub>
ZGNR [51]	DFT	H <sub>2</sub> S	−0.364
Pristine G (PG) [52]	DFT	SO <sub>2</sub>	−0.157
PG [49]	Exp. and MD	NH <sub>3</sub>	Not reported
PG [44]	DFT and MD	H <sub>2</sub>	Not reported
Graphene [48]	DFT	H <sub>2</sub> S	−0.038
		CH <sub>4</sub>	−0.022
DG (vacancy) [48]	DFT	H <sub>2</sub> S	−2.934
		CH <sub>4</sub>	−0.154
G-OH [48]	DFT	H <sub>2</sub> S	−1.263
		CH <sub>4</sub>	−0.047
Single layer G (SLG) [43]	Experimental	H <sub>2</sub>	Not reported
Bilayer G (BG) [53]	DFT	H <sub>2</sub> S	−0.360
		CH <sub>4</sub>	−0.086
		C <sub>2</sub> H <sub>2</sub>	−0.102
PG [54]	DFT	CO	−0.093
		NO <sub>2</sub>	[−0.214, −0.185]
PG [46]	DFT	H <sub>2</sub> S	[−0.201, −0.122]
		CO	−0.084
PG [55]	DFT	NO	−1.166
		CO	−0.069
		NO	−1.203
Vacancy G (VG) [55]	DFT	NO	[−0.1280, −0.1176]
		NO <sub>2</sub>	[−0.1679, −0.1427]
PG [56]	DFT	AsH <sub>3</sub>	Not reported
		CO	Not reported
PG [57]	DFT	H <sub>2</sub> S	−0.360
PG [58]	DFT	NO	[−2.3713, −1.7453]
PG supercell [47]	DFT	COCl <sub>2</sub>	−0.554
PG [59]	DFT	CO	−1.18
		CO <sub>2</sub>	−0.58
G nanoflakes (GNFs) [60]	DFT	CO <sub>2</sub>	−0.58

Table 2. Cont.

System	Type of Study	Adsorbate	$E_{ads}$
PG [45]	DFT	H <sub>2</sub> O	−0.047
		NH <sub>3</sub>	−0.031
		CO	−0.014
		NO <sub>2</sub>	−0.067
PG [42]	DFT	NO	−0.029
		H	[−0.84, −0.75]

### 2.3. Fullerenes

Fullerenes can be obtained directly from graphene [61]. They are the subject of a great deal of experimental and theoretical research due to their exciting adsorption properties given by their characteristics. From first-principles studies we know that the size of the fullerene impacts its stability and its hydrogen storage capacity. The cohesive and formation energies of fullerenes decrease with increasing size [62].

Furthermore, fullerenes adsorb gases like N<sub>2</sub>, Ar, and CO<sub>2</sub>, and for the latter, an exceptionally large C<sub>460</sub> fullerene would adsorb up to 28 wt% at room temperature [62]. A P-doped fullerene can adsorb the CO<sub>2</sub> molecules; such doping increases the selectivity of CO<sub>2</sub> concerning an N<sub>2</sub>/CO<sub>2</sub> mixture, as shown by DFT studies. Additionally, an electric field applied to the systems affects the interaction between the P-doped-CO<sub>2</sub> and the CO<sub>2</sub> molecule, going from physisorption to chemisorption [63].

Monte Carlo simulations show that C<sub>60</sub> fullerenes can also adsorb ethylene (C<sub>2</sub>H<sub>4</sub>) at 150 K [64]. Experimental results show that self-assembled C<sub>60</sub> crystals have excellent sensing properties to detect toxic aromatic solvent vapors such as aniline, toluene, benzene, ethanol, hexane, cyclohexane, and methanol [65].

Additionally, DFT studies showed that fullerene-based devices reduced nitrous oxide (N<sub>2</sub>O) and carbon monoxide (CO) pollution. In that case, Si-coordinated nitrogen-doped C<sub>60</sub> fullerenes, labeled as Si@C<sub>54</sub>N<sub>4</sub>, catalyzes the N<sub>2</sub>O reduction and CO oxidation in the presence of an O<sub>2</sub> molecule [66]. In [67], the authors found that metal oxides (MOx) such as Cu<sub>2</sub>O, ZnO, and NiO, when adsorbed on C<sub>60</sub> fullerenes, can adsorb nitrogen dioxide (NO<sub>2</sub>) as well as CO much better than C<sub>60</sub> alone. This is caused by a more significant charge transfer, more considerable adsorption energies, and more extensive enthalpy changes when compared to those of the pristine C<sub>60</sub> fullerene.

Such pristine C<sub>60</sub> fullerenes can adsorb H<sub>2</sub>, and their interaction has been studied by several means, including a modification of the L-J potential and the continuum approach [68]. When C<sub>60</sub> fullerenes oxidize at 400 °C and a pressure of 2 bar, they enhance their surface and increase H<sub>2</sub> adsorption. Experimental studies showed that this process increases the H<sub>2</sub> adsorption by a factor of three, at 77 K and a pressure of 120 bar [69]. When C<sub>60</sub> or C<sub>70</sub> fullerenes are doping helium droplets, they can physisorb both hydrogen H<sub>2</sub> and deuterium D<sub>2</sub> [70]. Furthermore, in [62], the authors showed that the previously mentioned C<sub>460</sub> fullerene would reach H<sub>2</sub> storage of 7.60 wt% at 300 K.

There are theoretical investigations to compare the efficiency of the porous structure of fullerenes with that of similar hexagonal boron nitride (hBN) nanocages. In [71], the authors showed that a B<sub>16</sub>N<sub>16</sub> fullerene-like form would have low conductivity and reactivity compared with the fullerene C<sub>32</sub> and a B-doped fullerene labeled as B<sub>8</sub>C<sub>24</sub>. They concluded that the B<sub>16</sub>N<sub>16</sub> system was the most suitable H<sub>2</sub> adsorbent of these three cases.

Other theoretical calculations using DFT show the adsorption of nitrogen gas (N<sub>2</sub>) molecules by different fullerenes such as sphere-like C<sub>82</sub> or the tubelike C<sub>110</sub>. The interaction between N<sub>2</sub> and such fullerenes can lead to (N<sub>2</sub>)<sub>n</sub> molecular clusters [72]. Similar studies show that NO and NO<sub>2</sub> molecules can be better adsorbed by a C<sub>60</sub> fullerene when the latter is B-, N-, or BN-codoped. The best adsorption performance is obtained with the BN-codoped C<sub>60</sub> fullerene, labeled as C<sub>58</sub>BN, and obtained after doping by substitution of two carbon atoms by nitrogen and boron atoms [73].

There are clusters formed with rare gas atoms with  $C_{60}XN$  where  $X = Ne, Ar, Kr, \text{ or } Xe$ . A study using an empirical approach to the potential energy surface explored the  $X-C_{60}$  and  $X-X$  interactions, showing that there is generally an energetically favorable cluster formation, with  $N$  ranging from 32 for  $Xe$  up to 60 for  $Ne$  [74]. By itself, a  $C_{60}$  fullerene can also adsorb  $He$  molecules [68].

The detection and sensing of chemical warfare agents (CWAs) is a research line where fullerenes play a relevant role. The tabun nerve agent ( $C_5H_{11}N_2O_2P$ ), a highly toxic and dangerous gas, is an example of this, as DFT calculations have shown that a  $C_{20}$  fullerene can adsorb it. Doping the fullerene with either boron or nitrogen affects its interaction with Tabun, showing that the B-doped fullerene, or  $C_{19}B$ , is better to detect the hazardous gas, due to a larger change of the system's electrical conductivity [75].

Cyanogen ( $C_2N_2$ ) is another toxic gas that fullerenes could detect. DFT/B3LYP calculations show that OH-functionalizing or Ge-doping of  $C_{60}$  fullerene result in a larger adsorption capacity than a pristine  $C_{60}$  fullerene, although the increase is relatively small [76]. Experimental investigations show that  $C_{60}$  fullerenes can adsorb the amphetamine (AA) drug. Additionally, DFT calculations show that the AA- $C_{60}$  interaction increases the fullerene by substituting C atoms with either Si or Ge atoms. In both cases, the AA drug tends to be adsorbed at the (6, 6) bonds of the  $C_{60}$  structure, i.e., the bonds joining two hexagons in the fullerene structure [77].

At a larger scale, fullerenes help to detect and adsorb industrial waste. For instance, a functionalized magnetic fullerene nanocomposite (FMFNC) obtained employing a thermal decomposition of polyethylene terephthalate (PET) bottles (environmentally convenient decomposition) is an excellent candidate to purify dye-contaminated wastewater [78]. Table 3 shows the main quantitative results of this section.

**Table 3.** Summary of adsorption energies  $E_{ads}$  (in eV) for different non-metallic doped fullerene systems and adsorbates. The type of study is also specified.

System	Type of Study	Adsorbate	$E_{ads}$
$C_{60}$ [70]	Exp. and DFT	$H_2$	[0.0495, 0.0641]
$C_{60}$ [74]	PES (potential energy surface)	Ne, Ar, Kr, Xe	Not reported
$C_{60}$ [69]	Experimental	H	-0.0247
$C_{60}$ [72]	DFT	$N_2$	[-0.28, -0.03]
$C_{60}$ [64]	GCMC	$C_2H_4$	[-0.0207, 0.0207]
$C_{60}$ [79]	DFT	CO	-0.006
$C_{60}$ [76]	DFT	NO	0.00008
$C_{60}$ [76]	DFT	$C_2N_2$	-4.78
OH- $C_{60}$ [76]	DFT	$C_2N_2$	-5.13
$C_{60}$ [77]	DFT	$C_9H_{13}N + N$	-0.017
$C_{60}$ [77]	DFT	$C_9H_{13}N + H$	-0.0516
$C_{32}$ [71]	DFT	$H_2$	[-0.118, -0.0086]
$C_{60}$ [65]	Experimental	Aromatic vapor	Not reported
$C_{60}-N_x$ [73]	DFT	NO	[-0.35, -0.28]
$C_{24} + P + N_{24}$ [80]	DFT	$NO_2$	[-1.01, -0.94]
$C_{60}+P$ [63]	DFT	$CO_2$	[-0.94, -0.30]
$Si@C_{54}N_4$ [66]	DFT	$CO_2$	[-1.97, 0.06]
$Si@C_{54}N_4$ [66]	DFT	$N_2O$	[-3.50, -0-77]
$Si@C_{54}N_4$ [66]	DFT	CO	[-3.50, -0-77]
$C_{60}$ [67]	DFT	$O_2$	-0.169
$C_{60}$ [67]	DFT	$N_2O$	-0.092
$C_{20}$ [75]	DFT	CO	[-0.054, -0.043]
B- $C_{20}$ [75]	DFT	$C_5H_{11}N_2O_2P$	[-1.092, -0.072]
N- $C_{20}$ [75]	DFT	$C_5H_{11}N_2O_2P$	[-0.027, -1.65]
$C_{460}$ [62]	DFT	$H_2$	-4.37
$C_{60}$ [68]	Modified LJ-potential	$CO_2$	[-0.49, -0.42]
$C_{60}$ [68]	Modified LJ-potential	$H_2, He$	Not reported



#### 2.4. Graphdiyne

Graphdiyne—in some works abbreviated as GDY—is a recently developed 2D material that has raised interest because it is a metal-free catalyst for low-temperature CO oxidation. It is helpful to absorb CO molecules. According to spin-polarized DFT calculations, graphdiyne can also absorb O<sub>2</sub> and does it more quickly than CO adsorption [81]. However, pristine graphdiyne does not capture N<sub>2</sub> efficiently [82].

In [83], the authors used DFT simulations and found that CO and methanol (CH<sub>3</sub>OH) are physisorbed by the pristine GDY surface, while a Ca-decorated graphdiyne (Ca-GDY) can further increase their adsorption. Ca-GDY can adsorb up to 29.81 wt% of CH<sub>3</sub>OH and 27.10 wt% of CO.

A GDY monolayer also adsorbs atomic oxygen and hydrogen at different sites. Hydrogen chemisorbs above a carbon atom and oxygen at the hollow place. According to such studies, oxygenated graphdiyne could be useful for spintronic devices [84].

Graphdiyne is helpful to detect amino acids, such as glycine (C<sub>2</sub>H<sub>5</sub>NO<sub>2</sub>), glutamic acid (C<sub>5</sub>H<sub>9</sub>NO<sub>4</sub>), histidine (C<sub>6</sub>H<sub>9</sub>N<sub>3</sub>O<sub>2</sub>), and phenylalanine (C<sub>9</sub>H<sub>11</sub>NO<sub>2</sub>). MD simulations at room temperature suggest that graphdiyne adsorbs such amino acids with an energy more significant than that on graphene, with dispersion interactions predominating in the process [85]. Graphdiyne can also adsorb dimethylamine (DMA) and—to a lesser level—trimethylamine (TMA) vapor molecules and desorb them in a short time, making it suitable for sensing devices [86].

Other studies show that graphdiyne is a helpful drug delivery agent for medical applications. DFT and Quantum-Monte-Carlo simulations suggest that GDY adsorb the drugs sorafenib (C<sub>21</sub>H<sub>16</sub>ClF<sub>3</sub>N<sub>4</sub>O<sub>3</sub>) and regorafenib (C<sub>21</sub>H<sub>15</sub>ClF<sub>4</sub>N<sub>4</sub>O<sub>3</sub>) then release them upon protonation [87].

Graphdiyne sheets adsorb ammonia molecules (NH<sub>3</sub>) according to ab initio calculations, showing a better adsorption capacity than graphdiyne nanotubes [88]. Formaldehyde (HCHO) and formic acid (HCOOH) in vapor form can also be adsorbed on the top, ring and bridge sites of a graphdiyne nanosheet [89].

Functionalizing hydrogen-substituted GDY nanostructures with pyridinic nitrogen enhances its electrocatalytic performance for oxygen reduction. Hydrogen-substituted graphdiyne (HsGDY) results from bonding hydrogen to three of the C atoms in a benzene ring, facilitating nitrogen doping [90]. HsGDY and B-decorated HsGDY has also been able to physisorb several gas molecules such as NO, NO<sub>2</sub>, NH<sub>3</sub> and N<sub>2</sub>. The optimal adsorption positions for these cases were located in the vicinity of the GDY benzene rings. The B-decorated HsGDY had a better adsorption performance, in particular for NO and NO<sub>2</sub> [91]. Boron decoration on a regular graphdiyne layer (BGDY) has also been considered as a possible electronic sensor for anticancer drugs like temozolomide (TMZ). The B decoration was also shown to increase the TMZ adsorption capabilities of GDY, related to an increase in its electrical conductivity of around 40%, according to ab initio calculations [92]. The 5-fluorouracil (5FU) anti-cancer drug—which shows no interaction with pristine GDY—can also be adsorbed by a BGDY composite, increasing the latter's electrical conductivity by around 25%, a feature that would make BGDY suitable for 5FU sensing [93].

Besides boron, other nonmetal atoms like Si, P, S, As, Se, and Te are used through DFT calculations to decorate graphdiyne surfaces to increase their ability to dissociate molecular oxygen. The As-, Se- and Te-decorated GDY monolayers physisorbed the O<sub>2</sub> molecule, while the B, N, O, Si, P, and S-decorated GDY chemisorbed it [94].

Li, an alkali metal, is another exciting option. The authors in [95,96] showed that this metal catalyzes the adsorption properties of graphene or carbon nanotubes. Studies have compared DFT-PBE and hybrid DFT+LC- $\omega$ PBE calculations to explore the Li adsorption on graphdiyne. PBE tends to overestimate the adsorption energy, suggesting that hybrid DFT should be preferred when studying GDY electronic properties [97]. Similar studies, including Li-decorated GDY, or Li@GDY, show that it could capture CO<sub>2</sub> molecules while investigating the possible conversion of CO<sub>2</sub> into beneficial—or at least less nocive—chemicals via carbon dioxide electrochemical reduction reaction (CO<sub>2</sub>RR) [98].

In [99], the authors found that CO<sub>2</sub>RR improved with nitrogen doping on graphdiyne (NGDY), increasing the selectivity regarding the doping with CH<sub>3</sub>OH and CH<sub>4</sub>. In particular, the lowest limiting potential of CH<sub>3</sub>OH on NGDY gets reduced. Further composites such as boron- and nitrogen-doped GDY anchoring a single Cu atom (labeled as Cu@N- and Cu@B-doped GDY) have also been systematically explored via ab initio calculations. The result is that Cu@N-doped GDY monolayers are more efficient than the boron-doped ones for CO<sub>2</sub> reduction and highly catalytic activity toward CO<sub>2</sub>RR [100].

However, there are cases where boron-doped GDY shows a better performance than nitrogen-doped GDY, as demonstrated by spin-polarized DFT studies. For instance, B-GDY shows excellent sensitivity and selectivity toward NO, NO<sub>2</sub>, and ammonia (NH<sub>3</sub>) [101]. Recently, a DFT study combining boron and nitrogen doping—a BN co-doping labeled as BN@GDY—of defective graphdiyne showed that it could increase the catalytic efficiency compared with boron doping alone. The increment in catalytic efficiency would be by a change in the B hybridization from sp<sup>2</sup> to sp<sup>3</sup> caused by the introduction of N atoms [102].

Improving catalysis can be seen the other way around: instead of decorating graphene sheets, they could be the decoration. For instance, when placed on the Pt(111) surface, a graphdiyne layer gives better results at increasing the latter two-dimensional confined catalysis performance compared with graphene or hexagonal boron nitride [103].

Finally, an increasing interest in the effective detection of chemical warfare agents (CWAs) has led to the investigation of graphdiyne as a possible sensor. Using ωB97XD DFT and Quantum theory of atoms in molecule (QTAIM) analysis, studies in [104] found that G-type nerve agents like GA(tabun), GB(sarin), GD(soman), and GF(cyclosarin) can be physisorbed at the triangular section of a GDY nanosheet. The GDY surface shows a short recovery time at room temperature, suggesting it can be a good option for sensor devices. Highly nocive A-series CWAs can also be physisorbed by GDY nanoflakes via noncovalent adsorption, as per DFT-ωB97XD calculations that consider long-range interactions [105]. Lewisite molecules are another type of toxic CWAs that DFT calculations show can be adsorbed by graphdiyne nanoflakes. In this case the study shows that GDY physisorbs Lewisite L<sub>1</sub>, L<sub>2</sub> and L<sub>3</sub> with the highest GDY sensitivity being found to be towards L<sub>2</sub> [106]. Table 4 shows the main quantitative results of this section.

**Table 4.** Summary of adsorption energies E<sub>ads</sub> (in eV) for different non-metallic doped graphdiyne systems and adsorbates. The type of study is also specified.

System	Type of Study	Adsorbate	E <sub>ads</sub>
GDY [86]	DFT	DMA	[−0.503, −0.757]
		TMA	[−0.607, −0.796]
		C <sub>2</sub> H <sub>5</sub> NO <sub>2</sub>	[−1.10, −0.59]
GDY supercell [85]	DFT	C <sub>5</sub> H <sub>9</sub> NO <sub>4</sub>	[−1.14, −0.54]
		C <sub>6</sub> H <sub>9</sub> N <sub>3</sub> O <sub>2</sub>	[−1.46, −0.73]
		C <sub>9</sub> H <sub>11</sub> NO <sub>2</sub>	[−1.53, −0.77]
GDY, BGDY [92]	DFT	TMZ	[−1.97, −0.95]
GDY nanoflakes [105]	DFT	CWA A-230	−0.594
		CWA A-232	−0.713
		CWA A-234	−0.745
GDY [81]	DFT	CO	−1.43
		O <sub>2</sub>	−3.27
GDY-NS [87]	DFT	C <sub>21</sub> H <sub>16</sub> ClF <sub>3</sub> N <sub>4</sub> O <sub>3</sub>	[−0.660, −0.085]
		C <sub>21</sub> H <sub>15</sub> ClF <sub>4</sub> N <sub>4</sub> O <sub>3</sub>	[−0.641, −0.081]
GDY [89]	DFT	CH <sub>2</sub> O	[−1.502, −0.342]
		CH <sub>2</sub> O <sub>2</sub>	[−0.945, −0.390]
GDY [107]	DFT	Ag	[−0.792926, −1.236]
		Cu	[−0.622651, −2.783]
		Ni	[−2.913467, −3.446]
		Zn	[−0.0196, 0.0356]
GDY [84]	DFT	H	−3.73
		O	−7.53

Table 4. Cont.

System	Type of Study	Adsorbate	$E_{ads}$
GDY nanoflakes [106]	DFT	$L_1$	−0.441
		$L_2$	−0.534
		$L_3$	−0.567
GDY [97]	Hybrid DFT	Li	−1.82
Ca-GDY [83]	DFT	$CH_4O$	[−0.349, −0.122]
		CO	[−0.128, −0.060]
GDY [104]	DFT, QTAIM	CWA GA	−0.707
		CWA GB	−0.520
		CWA GD	−0.543
		CWA GF	−0.382
GDY [88]	DFT	$NH_3$	[−0.465, −0.435]
GDY [108]	DFT	Pd clusters	[−4.0, −3.0]

### 2.5. Hybrid Systems

We define a hybrid system as the surface created using different carbon nanostructures, i.e., the combination of graphene or graphdiyne with nanotubes or fullerenes or semi fullerenes or buckybowls. The result is a set of structures with a larger specific area for gas adsorption purposes. For instance, theoretical investigations use DFT focused on the hydrogen adsorption on a system made of graphene decorated with  $C_{176}$ . The results show that the adsorption energies ranged between 0.069 and 0.115 eV. Up to four hydrogen molecules could get into the  $C_{176}$  [109].

Another frequently investigated structure for gas adsorption is pillared graphene, which comprises graphene sheets joined by carbon nanotubes. In [110], the authors investigated the hydrogen storage capacity in pillared graphene using MD calculations to study the effects of the environment's pressure, temperature, and geometric structure. They found that pillared graphene has a higher performance than CNTs as a hydrogen storage material, a fact that due to its larger surface area.

Using a hybrid molecular dynamics–Monte Carlo simulation method, the authors in [111] investigated the methane ( $CH_4$ ) adsorption on Pillared graphene. They found that in this case, the CNT length has the most significant effect on the adsorption amount of methane among different geometrical parameters such as CNT diameter, graphene sheet layer spacing, and the number of CNTs. The adsorption ability of pillared graphene is greater than that of graphene sheets. Such a structure has higher mechanical stability than graphene.

A variation of the pillared graphene system considers fullerenes instead of nanotubes placed between the graphene sheets. In [112], the authors considered this variation and studied methane adsorption with adjustable micro and mesoporous morphology. Their simulations via grand canonical Monte Carlo simulations revealed that this system is suitable for methane storage. Other studies performing similar simulations have explored the same kind of nanostructure for hydrogen adsorption [113]. They considered three different fullerenes such as  $C_{180}$ ,  $C_{320}$ , and  $C_{540}$ . Hence, this would be a potentially helpful system for hydrogen storage.

Other studies involving grand canonical Monte Carlo simulations considered fullerenes placed between graphene sheets and lithium doping to investigate methane ( $CH_4$ ) adsorption. These structures are labeled as Sandwiched Graphene-Fullerene Composite (SGFC) and have a promising potential for methane storage applications. This Li-doped nanostructure could be considered suitable host materials for lightweight methane storage devices [112]. The same SGFC, both undoped and Li-doped, has been explored in terms of its hydrogen adsorption capacity. Employing grand canonical Monte Carlo calculations, three fullerene types as the sandwich core have also been studied:  $C_{180}$ ,  $C_{320}$ , and  $C_{540}$ . It was observed that a Li-doped nanostructure with a doping ratio of Li:C = 1:8 can overpass the gravimetric capacity of 5%, while an undoped one can reach the value of 3.83% at 77 K

and 1 bar. The Li-doped SGFC capacity is larger than that observed in graphene-based systems [113].

Carbon nano onions (CNO) are another interesting mixed nanostructure discovered in 1992. These systems are multi-shell fullerenes with concentric shells of carbon atoms with an interlayer distance similar to graphite [114]. Experimental investigations on the synthesis of hollow carbon nano-onions and their use for adsorbing hydrogen molecules showed that the hollow CNOs exhibit good performance as materials for electrochemical hydrogen storage. Furthermore, using DFT calculations, the authors in [115] studied the properties of stoichiometric and defective nitrogen carbon nano onions, or NCNOs. Exploring the stability and thermodynamic properties of mono and divacancy-containing CNOs showed that the latter is more stable and can increase the bandgap notably.

To finish this section, we will focus on buckybowls. A buckybowl is not a hybrid system, but an interesting one nevertheless. These structures come from the fragmentation of fullerenes. Buckybowls are adsorbents of CO<sub>2</sub>, CH<sub>4</sub>, and C<sub>2</sub>H<sub>2</sub>. Studies using hybrid DFT calculations found that the curvature of the buckybowl surface plays a significant role in the adsorption of these gas molecules. Buckybowls are high-performance materials for capturing greenhouse gases, molecular recognition, and nanotechnology applications in general [116]. Hybrid nanostructures can also see their adsorption capacity increase by doping them, usually with lithium and nitrogen as dopants. Table 5 shows the main quantitative results of this section.

**Table 5.** Summary of adsorption energies  $E_{\text{ads}}$  (in eV) for different non-metallic doped hybrid systems and adsorbates. The type of study is also specified.

System	Type of Study	Adsorbate	$E_{\text{ads}}$
CNO [117]	Experimental	H <sub>2</sub> O	Not reported
CNO [115]	DFT	mN, m = 1–10	[−0.18, 0.33]
Buckybowls [116]	Hybrid-DFT	CO <sub>2</sub> , CH <sub>4</sub> , C <sub>2</sub> H <sub>2</sub>	Not reported
C <sub>20</sub> , C <sub>20</sub> (bowl) [118]	DFT	N, H	Not reported
Nanobuds [109]	DFT	H <sub>2</sub>	[0.069, 0.115]
Sandwiched G-fullerene + Li [113]	GCMC	H <sub>2</sub>	Not reported
Pillared-graphene [110]	MD	H <sub>2</sub>	Not reported
Fullerene pillared-graphene [112]	GCMC	CH <sub>4</sub>	Not reported
Pillared-graphene [111]	GCMC-MD	CH <sub>4</sub>	Not reported

### 3. Adsorption on Systems Doped with Transition Metals

#### 3.1. Transition Metals

The definition of transition metals usually refers to those elements in groups 3–12 on the periodic table, with partially filled d-orbitals. The frequent name for the lanthanide and actinide series is inner transition metals. However, it is more frequent to call transition metals the elements of groups 4–11. This fact relies on the typical chemical behavior of the metals in these groups. Note that the filling of the d-orbitals increases going from left to right in the periodic table. It is usual to name them the “d-block elements.” Thus, these metals have several properties in common. First, they have low ionization energies, and several of them form paramagnetic compounds. Second, these metals are reactive but not as much as the alkalis. Finally, they conduct heat and electricity very well and have high melting and boiling temperatures.

#### 3.2. Nanotubes Doped with Transition Metals

Doping nanotubes to increase their adsorption capacity is frequent. In particular, the decoration involving transition metals, oxides, or polymers, can increase their sensitivity [119]. It is also frequent to use transition metals Pd, Pt, Ag, Au, and Rh for doping carbon nanotubes that in turn can be used as gas sensors [31,120–136] for detection of gases of C<sub>3</sub>H<sub>6</sub>O (acetone), C<sub>6</sub>H<sub>6</sub> (benzene), H<sub>2</sub>, CH<sub>4</sub>, NH<sub>3</sub>, NO<sub>2</sub>, H<sub>2</sub>O, CO, H<sub>2</sub>S, HCN, HCl, Cl<sub>2</sub>. Specifically, Pd used for the adsorption of H<sub>2</sub>, Cl, CH<sub>4</sub>, Cl<sub>2</sub>, acetone, benzene; Pt used for

the adsorption of C<sub>7</sub>H<sub>8</sub> (toluene), H<sub>2</sub>, NO<sub>2</sub>, H<sub>2</sub>O, NH<sub>2</sub>; Au for the adsorption of C<sub>2</sub>H<sub>6</sub>O (ethanol), NH<sub>3</sub>, NO<sub>2</sub>, and Rh used for the adsorption of HCl, CO, and CH<sub>4</sub>. Furthermore, doping with Fe makes adsorption of the hydrogen molecule stronger than on an undoped nanotube. The adsorption of Fe on the nanotube is exothermic [137].

Experimental studies found that the H<sub>2</sub> storage capacity of pristine MWCNTs increases up to 15 times at room temperature and 2.0 MPa by decorating them with ultrafine Ti nanoparticles. This improvement does not affect the cyclic hydrogenation–dehydrogenation operation of the tubes [138]. The intercalation of nickel on MWCNTs increases the H<sub>2</sub> adsorption, probably due to the strong interaction between the Ni atoms and the MWNTs [139].

DFT calculations of Pt-decorated nanotubes show different effects in the adsorption capacities of the latter. For instance, the nanotube conductivity can vary with the adsorption of H<sub>2</sub>S, CO, and SO<sub>2</sub> [140]. Another DFT calculation shows that Au-decorated nanotubes have a high sensitivity to adsorption of SO<sub>2</sub> and H<sub>2</sub>S [141]. These Au-decorated nanotubes help sense propanone or acetone (C<sub>3</sub>H<sub>6</sub>O) gas, with the Au decoration increasing the device sensitivity up to around 3% at room temperature [142].

Rh-doped single-walled carbon nanotubes are advantageous for the adsorption of CO, C<sub>2</sub>H<sub>4</sub> (ethylene), and SO<sub>2</sub> molecules while proving to be insensitive to CO<sub>2</sub> and CH<sub>4</sub> [143]. DFT calculations using dispersion corrections in [144] showed that the doping of a (14,0) carbon nanotube by substituting a carbon atom with a Ru atom conveys better adsorption of SO<sub>2</sub> and H<sub>2</sub>S molecules by the Ru-doped SWNT.

Pd and Pt decorations on a nanotube are practical to adsorb CO and NO molecules. Pd decoration is more suitable to adsorb NO, while Pt works better for CO adsorption. Ab initio calculations showed that this adsorption would change the magnetic properties of the Pd- and Pt-decorated SWCNTs, which would be helpful for sensors [145].

Pd as a dopant facilitates the adsorption of N<sub>2</sub>O on the otherwise inert nanotube [146]. More DFT calculations predict that Rh-doped nanotubes present a good adsorption ability of O<sub>2</sub> and O<sub>3</sub> and show relatively significant conductivity changes [147]. There is experimental evidence that Au nanoparticles adsorbed on nanotubes are helpful for acetone gas sensing at room temperature [148].

Table 6 presents a list of transition metals used for doping carbon nanotubes and the gases adsorbed in the doped nanotube. Notice that the most used is Au, and the least used are Ag and Fe. From the 32 elements in the periodic table (groups 4–11), we found mainly six transition metals used as dopants. Table 7 shows the main quantitative results of this section.

**Table 6.** List of transition metals used for doping carbon nanotubes and the corresponding adsorbed gases.

Metal	Adsorbed Molecules
Ag	NO <sub>2</sub> [133]
Au	NH <sub>3</sub> , NH <sub>2</sub> [132,133,135]; SO <sub>2</sub> , H <sub>2</sub> S [141]; C <sub>2</sub> H <sub>6</sub> O [31]; C <sub>3</sub> H <sub>6</sub> O [142,148]
Pt	H <sub>2</sub> , NO <sub>2</sub> , H <sub>2</sub> O, NH <sub>3</sub> [132]; C <sub>7</sub> H <sub>8</sub> [136]; NO [145]
Pd	H <sub>2</sub> [120–125,128]; NO <sub>2</sub> [135], Cl <sub>2</sub> [135]; CH <sub>4</sub> [126,127]; NO [145]; N <sub>2</sub> O [146]
Fe	H <sub>2</sub> [137]
Rh	CO [134]; CO, C <sub>2</sub> H <sub>4</sub> SO <sub>2</sub> [143]; O <sub>2</sub> , O <sub>3</sub> [147]

**Table 7.** Summary of adsorption energies  $E_{\text{ads}}$  (in eV) for different TM-doped nanotubes systems and adsorbates. The type of study is also specified.

System	Type of Study	Adsorbate	$E_{\text{ads}}$
CNT(APTS) [18]	Experimental	CO <sub>2</sub>	Not reported
Fe-SWCNTs [137]	DFT	H <sub>2</sub>	[−0.238, −0.141]
Au-CNTs [31]	Experimental	C <sub>2</sub> H <sub>6</sub> O	Not reported
Pt-SWCNTs [140]	DFT	SO <sub>2</sub>	−1.225
		H <sub>2</sub> S	−0.977
		CO	−1.386
Au-SWCNTs [141]	DFT	SO <sub>2</sub>	−1.258
		H <sub>2</sub> S	−1.317
Au-CNTs [142]	Experimental	C <sub>3</sub> H <sub>6</sub> O	Not reported
		CO	[−3.527, −1.308]
Rh-CNT [143]	DFT	CO <sub>2</sub>	−0.348
		CH <sub>4</sub>	−0.253
		C <sub>2</sub> H <sub>4</sub>	−1.189
		SO <sub>2</sub>	−1.158
		CO	[−1.8, −1.6]
Pd-, Pt-SWNTs [145]	DFT	NO	[−1.814, −1.46]
		N <sub>2</sub> O	−0.91
Pd-CNT [146]	DFT	O <sub>2</sub>	−1.384
		O <sub>3</sub>	[−2.711, −1.824]
Pt-MWCNTs [136]	Experimental	C <sub>7</sub> H <sub>8</sub>	Not reported
Au-CNTs [148]	Experimental	C <sub>3</sub> H <sub>6</sub> O	Not reported
Pd-, Pt-, Rh-, Au-SWNTs [134]	Experimental	H <sub>2</sub> , CH <sub>4</sub> , CO, H <sub>2</sub> S	Not reported

### 3.3. Graphene Doped with Transition Metals

We label TM-doped graphene the graphene doped with transition metals in this review. As with the other nanostructures considered in this review, hydrogen adsorption is a heavily explored topic, and transition metal-doped graphene has been no exception. For instance, a TiO<sub>2</sub> decoration of nanoparticles on graphene oxide (GO + Ti) can adsorb twice as much H<sub>2</sub> as pristine graphene at room temperature and 5 MPa, showing reversibility of up to 80% [149]. Copper-decorated N-doped defective graphene nanoribbons can improve their reactivity towards H<sub>2</sub> adsorption. In [150], a DFT study considered single vacancy defects on graphene doped with N atoms, forming a pyridine-like structure. The authors labeled these structures as SV+1N, SV+2N, or SV+3N, depending on the number of nitrogen atoms. They added Cu decoration on each resulting system and concluded that the Cu-decorated SV+3N showed the best H<sub>2</sub> adsorption performance, with a promising reversible cycle.

TM-doped graphene has been considered a possible candidate to sense different polluting gases, which usually interact weakly with pristine graphene. We have the chemical warfare agents (CWAs) among the pollutant gases under investigation, mentioned in Section 2.3. Transition metals such as Zr, Mo, Ti, Mn, Fe, and Co dope graphene and increase adsorption capabilities. For instance, Mn-doped graphene shows the most substantial chemical adsorption of phosgene (COCl<sub>2</sub>), a highly toxic CWA [59].

Other DFT studies suggest that Mn-doped graphene substantially improves the adsorption of C<sub>2</sub>H<sub>2</sub>, CH<sub>4</sub>, and CO, which are characteristic dissolved gases in transformer oil. In [54], the authors found that this substrate would be appropriate for sensing only the first two gases mentioned. The adsorption of CH<sub>4</sub> is weak due to an electronic hybridization.

TM-doped graphene with TM = Ni, Cu, Zn, or Ni-doped vacancy defect graphene (DG) and graphene oxide (G-OH) adsorb hydrogen sulfide (H<sub>2</sub>S) that is another toxic and colorless gas. DFT studies show that Cu-doped graphene and DG display the best performance to adsorb H<sub>2</sub>S among the cases considered. Ni and Zn-doped graphene show weaker adsorption energies. Other studies show that Pt-decorated graphene is an H<sub>2</sub>S detector. The most stable configuration for adsorption corresponds to the H atoms of

the H<sub>2</sub>S pointing towards the TM-doped graphene [46,48,58]. The bilayer graphene (BG) adsorbs H<sub>2</sub>S, and this adsorption increases by doping (BG) with transition metals as Fe, Ni, Mn, Cr, Co, and V. Notice that the TM-doping can occur at more sites concerning a single graphene layer, for example, in the interlayer region.

DFT calculations also show that an external electric field would further increase the adsorption of H<sub>2</sub>S onto such TM/BG systems. As most TM/BG-H<sub>2</sub>S systems have semiconductor behavior, this could also be a good candidate for sensing devices [53]. Additionally, the H<sub>2</sub>S sensing performance of zigzag graphene nanoribbons (ZGNR) is also increased mainly by combined doping of Cu and Zn atoms, the resulting system labeled as Cu/Zn-ZGNR, with a high response value of around 49% [51].

TM-doped graphene (with TM = Ti, Mn, Fe, Co, Ni, and Ag) adsorbs arsine (AsH<sub>3</sub>), another toxic gas. As in previous cases, TM doping increases the chemical interaction with the gas compared with pristine graphene. In [57], the authors found that Ni-doped graphene has the best AsH<sub>3</sub>/CO selectivity, an important feature when removing arsine from CO gas streams. The resulting hybridization of states between AsH<sub>3</sub>, CO, and TM orbitals confirmed the chemical interaction.

Recent theoretical investigations utilizing DFT considered Ag- Pt- and Au-doped graphene as a possible sensing material of nitrogen oxides such as NO and NO<sub>2</sub>. Au-doped graphene shows the best adsorption performance of NO/NO<sub>2</sub> molecules of the three transition metals considered. Ag/Pt/Au-doping generally gives better sensing results than non-TM doping like B, N, Al, or S [56]. In [151], from DFT simulations, the authors found that Fe-doped graphene shows a high NO<sub>2</sub> adsorption rate due to the d-orbital impurity states from the metal on the graphene surface. They also found that an increase in the strain applied to the graphene sheet decreases its adsorption capacity. Fe-doped armchair graphene nanoribbons (Fe-AGNR) are candidates for NO and NO<sub>2</sub> sensing devices due to their electronic and transport properties [152].

Group 10 transition metals such as Ni, Pd and Pt can also decorate graphene to increase its interactions with NO<sub>2</sub> [46] significantly. Of the same group 10, palladium is another exciting option for graphene doping. It has been shown via DFT calculations that Pd-doped graphene can adsorb CO and NO molecules, with the most stable site being a bridge site (B-site). Pd doping vastly increases the interaction between the substrate and CO/NO [55].

Platinum clusters like the Pt<sub>13</sub> structure, when supported on pristine graphene, can also enhance the adsorption capacity of the latter. A systematic DFT study showed that such a composite could adsorb CO<sub>2</sub>, NO<sub>2</sub>, and SO<sub>2</sub> more effectively than defective graphene (DG) supported Pt<sub>13</sub> [153].

The latter gas, sulfur dioxide, has also been the subject of experimental and theoretical studies involving TM-decorated graphene. SO<sub>2</sub> can be adsorbed more efficiently by metal-oxide such as ZnO, BeO, and Ni-decorated graphene than pristine graphene. ZnO- and BeO-decorated graphene physisorb SO<sub>2</sub>, while Ni-decorated graphene chemisorbs it [52].

TM-doped graphene can also enhance the detection of formaldehyde (HCHO) gas. A first-principles study considered a two-probe sensor device built with TM-doped graphene, where TM = Co, Ni, Cu, Zn, Pd, and Ag. The Cu- and Ag-doped graphene devices showed the best performance at low voltages, with a short response time and high HCHO sensing [154]. Table 8 shows the main quantitative results of this section.

**Table 8.** Summary of adsorption energies  $E_{\text{ads}}$  (in eV) for different TM-doped graphene systems and adsorbates. The type of study is also specified.

System	Type of Study	Adsorbate	$E_{\text{ads}}$
Zn-ZGNR [51]	DFT	H <sub>2</sub> S	−2.237
Cu-ZGNR [51]	DFT	H <sub>2</sub> S	−1.129
Cu/Zn-ZGNR [51]	DFT	H <sub>2</sub> S	−7.043
Ni-G [52]	DFT	SO <sub>2</sub>	−2.297

Table 8. Cont.

System	Type of Study	Adsorbate	E <sub>ads</sub>
TM-PG [154] TM = Ti, V, Cr, Mn, Fe, Co, Ni, Cu, Zn, Pd, Ag, Pt, Au	DFT	HCHO	[0.83, 2.01]
Cu+1N-GNR [150]	DFT	H <sub>2</sub>	−0.020
Cu+2N-GNR [150]	DFT	H <sub>2</sub>	−0.200
Cu+3N-GNR [150]	DFT	H <sub>2</sub>	−0.780
TiO <sub>2</sub> -GO [149]	Experimental	H <sub>2</sub>	Not reported
Ni-G [48]	DFT	H <sub>2</sub> S	−0.699
		CH <sub>4</sub>	−0.099
TM-BG [53] TM = V, Cr, Mn, Fe, Co, Ni	DFT	H <sub>2</sub> S	[−0.58, −0.18]
Pt <sub>13</sub> -G [153]	DFT	CO <sub>2</sub>	[−4.217, −2.422]
		NO <sub>2</sub>	[−3.767, −2.586]
		SO <sub>2</sub>	[−3.260, −2.238]
Pt <sub>13</sub> -DG [153]	DFT	CO <sub>2</sub>	[−3.201, −0.916]
		NO <sub>2</sub>	[−3.345, −2.309]
		SO <sub>2</sub>	[−2.978, −2.065]
		CH <sub>4</sub>	−0.073
Mn-G [54]	DFT	C <sub>2</sub> H <sub>2</sub>	−2.424
		CO	−1.954
Ni-G [46]	DFT	NO <sub>2</sub>	[−2.631, −2.395]
		H <sub>2</sub> S	[−1.846, −1.811]
Pd-G [46]	DFT	NO <sub>2</sub>	[−1.586, −1.294]
		H <sub>2</sub> S	[−1.228, −1.224]
Pt-G [46]	DFT	NO <sub>2</sub>	[−2.003, −1.804]
		H <sub>2</sub> S	[−2.034, −1.858]
Pd-G [55]	DFT	CO	[−1.227, −0.909]
		NO	[−3.916, −1.308]
Ag-G [56]	DFT	NO	[−6.9262, −6.9101]
		NO <sub>2</sub>	[−7.8293, −7.7806]
Pt-G [56]	DFT	NO	[−6.2225, −6.1646]
		NO <sub>2</sub>	[−7.3758, −7.3723]
Au-G [56]	DFT	NO	[−8.4730, −8.3567]
		NO <sub>2</sub>	[−9.3391, −9.3209]
TM-G [57] TM = Ti, Mn, Fe, Co, Ni, Ag	DFT	AsH <sub>3</sub>	[−0.95, −1.45]
		CO	[−1.00, 2.02]
Ni-G [58]	DFT	H <sub>2</sub> S	−0.97
Cu-G [58]	DFT	H <sub>2</sub> S	−1.15
Zn-G [58]	DFT	H <sub>2</sub> S	−1.16
		CO <sub>2</sub>	[−0.89, −1.19]
TM-G [151] TM = Fe, Ni, Co, Cu	DFT	NO	[−0.68, −1.23]
		NO <sub>2</sub>	[−2.06, −2.57]
		SO <sub>2</sub>	[−0.89, −1.47]
		CO	−2.4
Fe- AGNR [152]	DFT	CO <sub>2</sub>	−1.3
		NO	−3.1
		NO <sub>2</sub>	−3.0
Zr-G [59]			−0.894
Mo-G [59]			−0.960
Ti-G [59]	DFT	COCl <sub>2</sub>	−1.065
Mn-G [59]			−1.677
Fe-G [59]			−1.378
Co-G [59]			−0.828
TM-GNF [60] TM = Sc, Ti, V, Cr, Mn, Fe, Co, N, Cu, Zn	DFT	CO	[−8.13, −37.56]
		CO <sub>2</sub>	[−5.05, −16.11]
MN <sub>4</sub> -G [155] M = Sc, Ti, V, Cr, Mn, Co, Ni, Cu, Zn	DFT	CO <sub>2</sub>	[−0.0032, −0.0125]



### 3.4. Fullerenes Doped with Transition Metals

The TM-doping or decoration increases the adsorption capacities of fullerenes. This increase by doping is present in the other carbon nanostructures reviewed in this work. In [79], the authors performed a systematic DFT study focused on TM decoration of C<sub>60</sub> fullerene, with TM = Ti, V, Cr, Mn, Fe, Co, Ni, Cu, and Zn. The changes in the electronic structure implied that the TM-decorated C<sub>60</sub> fullerene is more sensitive to CO and NO molecules than the pristine one.

Doping fullerenes with titanium increases their H<sub>2</sub> storage capacity. A way of doing it is by substituting carbon atoms with titanium atoms and doping a C<sub>60</sub> fullerene with an increasing number of Ti atoms, from one up to six. With six Ti atoms doping C<sub>60</sub> fullerenes in this fashion—labeled as Ti<sub>6</sub>C<sub>48</sub>—the hydrogen storage can be up to 7.7 wt% [156]. In [157], the authors performing DFT simulations found that Co atoms forming compact clusters on the surface of a C<sub>60</sub> fullerene labeled as C<sub>60</sub>Co<sub>n</sub>, chemisorb an H<sub>2</sub> molecule, with different features for different values of *n* (*n* = 1 to 8). They also found that up to 13 H<sub>2</sub> molecules could be absorbed in this way.

Theoretical calculations performed in [158] showed that a C<sub>70</sub> fullerene doped with TM ions (Cr<sup>2+</sup> and Co<sup>2+</sup>) adsorbed nitrogen dioxide (NO<sub>2</sub>) on the exterior surface. The doping mechanism is a porphyrin-induced process labeled as PIC70F. In this manner, this fullerene would be helpful for selective detection of NO<sub>2</sub> in the presence of sulfur dioxide, also showing a short recovery time.

Another way of doping fullerenes is from the inside, an example of which would be the endohedral metallofullerenes (EMFs). Such structures are obtained by putting a lowest energy structure of a metal cluster inside of the fullerene and then relaxing the system. When C<sub>60</sub> fullerenes are considered, the EMFs obtained in this manner are labeled as Mn@C<sub>60</sub>, and they can increase the oxygen reduction reaction (ORR) activities of the former. A comprehensive DFT study showed that EMFs such as Mn<sub>5</sub>@C<sub>60</sub>, Cu<sub>4</sub>@C<sub>60</sub>, Co<sub>2</sub>@C<sub>60</sub>, and Ni<sub>4</sub>@C<sub>60</sub> have better ORR activities, which could be helpful in developing sensing devices able to detect polluting gases [159]. Table 9 shows the main quantitative results of this section.

**Table 9.** Summary of adsorption energies E<sub>ads</sub> (in eV) for different TM-doped fullerene systems and adsorbates. The type of study is also specified.

System	Type of Study	Adsorbate	E <sub>ads</sub>
Ti-C <sub>60</sub> [156]	DFT	H <sub>2</sub>	−0.14
TM-C <sub>60</sub> [79] TM = Cr, Mn, Fe, Co, Ni, Cu; Zn	DFT	CO	[−2.94, −1.03]
		NO	[−6.52, −1.95]
		NO <sub>2</sub>	[−1.55, −0.605]
Cr-C <sub>70</sub> [158]	TD-DFT	SO <sub>2</sub>	[−1.178, −0.025]
Co-C <sub>70</sub> [158]	TD-DFT	NO <sub>2</sub>	[−1.919, −0.806]
		SO <sub>2</sub>	[−0.627, −0.0047]
M <sub>x</sub> -C <sub>60</sub> [159] M = Mn, Co, Ni, Cu (x = 2–5)	DFT	CH <sub>3</sub> OH	[−0.26, −0.17]
		HCOOH	[−0.19, −0.08]
		CH <sub>3</sub> CH <sub>2</sub> OH	[−0.27, −0.16]
		O <sub>2</sub>	[−0.19, −0.10]
		CO	[−0.35, −0.12]
Co <sub>n</sub> -C <sub>60</sub> [157] (n = 1–8)	DFT	SO <sub>2</sub>	[−0.22, −0.09]
		H <sub>2</sub>	[1.31, 0.60]
		2H	[1.78, 1.08]
TM-C <sub>60</sub> [67] TM = Cu, Zn, Ni	DFT	N <sub>2</sub> O	[−2.30, −1.41]
		CO	[−3.5, −1.56]

### 3.5. Graphdiyne Doped with Transition Metals

Transition metals (TMs) can enhance the adsorption properties of graphdiyne (GDY). Several DFT studies have explored the adsorption of metals like Au, Cu, Ni, and Zn—although Zn is not a transition metal—on graphdiyne. GDY strongly chemisorbs nickel,

and it also chemisorbs silver and copper. On the other hand, graphdiyne physisorbs a zinc atom. Overall, this material is better adsorbent for those metals compared with graphene [107]. When the GDY surface first adsorbs one or two nitrogen atoms, the resulting N-GDY composite increases the stability of further transition metal decorations. In [160], the authors investigated the adsorption of several TMs (Cr, Mn, Fe, Co, Ni, and Cu) on such N-GDY substrates. They found that Fe@2N-GDY (a Fe atom decorating a GDY doped with 2 N atoms) has the best catalytic activity with the lowest CO oxidation energy barrier.

As with the other nanostructures covered in this review, graphdiyne has been explored for its H<sub>2</sub> adsorption capabilities, aiming at reversible hydrogen storage. DFT studies have considered decorating graphdiyne nanosheets with light metals such as Li, Na, K, Ca, Sc and Ti. Some works have explored up to 11% of metal functionalization in the GDY surface, which can then anchor multiple H<sub>2</sub> molecules [161].

Water splitting is another exciting application of TM-decorated GDY nanosheets. For instance, theoretical simulations and experimental studies show that Ru-doped GDY (Ru/GDY) has a high catalytic performance for oxygen evolution reactions [162].

The electrochemical reduction of N<sub>2</sub> at room temperature is relevant for the production of ammonia (NH<sub>3</sub>). A systematic study considering transition-metal-embedded GDY, or TM@GDY, explored the effect of Sc, Fe, Cr, Mn, Mo, Co, Ni, Cu, Zn, Ru, Rh, Pd, and Ag in the N<sub>2</sub> reduction reaction. According to spin-polarized DFT simulations, the most stable and best catalytic activity was the Mo-embedded graphdiyne monolayer [163]. All TMs increase GDY sheets' N<sub>2</sub> reduction reaction (NRR) character. However, other studies indicate that the single-atom catalyst V@GDY monolayer has the best NRR performance [82].

Anchoring two transition metals to GDY improves the NRR activity. In a study involving DFT calculations, the authors considered several TMs (Fe, Co, Ni, Cu, and Mo). They found that the best NRR performance was with the Co-Ni heteronuclear complex (CoNi@GDY) and the Mo-Mo homonuclear complex (Mo<sub>2</sub>@GDY) [164].

Scandium and titanium can also decorate graphdiyne to enhance sensing of formaldehyde (HCHO), a typical air pollutant. Sc or Ti take a stable place on the corner sites of graphdiyne sheets, and both can better adsorb HCHO compared with pristine graphdiyne and graphene. This effect would be due to the electronegativity of HCHO, and the best result is with Ti-decorated graphdiyne, according to DFT calculations [165].

In [108], the authors investigated the palladium clusters supported on graphdiyne surfaces utilizing DFT calculations. They found that the electronic HOMO-LUMO gap changes with the size of said clusters, which chemisorbed with relatively high adsorption energies of around 3–4 eV in magnitude. Palladium nanoparticles can also be experimentally anchored to the GDY surface, forming a stable nanocatalyst labeled PdNPs/GDY. Such composite can decompose H<sub>2</sub>O<sub>2</sub> to produce O<sub>2</sub>, an essential reaction in antitumor treatments combined with doxorubicin, a chemotherapeutic agent [166].

Doping GDY with Fe atoms improves the electrochemical reduction of CO<sub>2</sub> by GDY sheets. An *ab initio* study found that doping the GDY surface with a Fe dimer or a Fe trimer optimizes the CO<sub>2</sub> adsorption and selectivity. The number of Fe atoms considered can generally tune the GDY catalytic activity significantly [167]. CO oxidation would also be accomplished employing several single-atom catalysts (SACs) such as Ni-GDY and Cu-GDY. DFT calculations have shown that both Ni and Cu can be anchored at the corner of the acetylenic ring of graphdiyne, the resulting system being able to adsorb CO [168]. Table 10 shows the main quantitative results of this section.

**Table 10.** Summary of adsorption energies  $E_{\text{ads}}$  (in eV) for different TM-doped graphdiyne systems and adsorbates. The type of study is also specified.

System	Type of Study	Adsorbate	$E_{\text{ads}}$
TM-GDY [98] TM = Li, Na, K, Rb, Cs	DFT	CO <sub>2</sub>	[−0.54, −0.21]
Cu-GDY [100]			[−0.5, −0.4]
Cu-B-GDY [100]	DFT	CO <sub>2</sub>	[−0.45, −0.3]
Cu-N-GDY [100]			[−0.5, −0.31]
Pt-GDY [103]	DFT	O <sub>2</sub>	−1.14
		CO	−1.56
		O <sub>2</sub>	−0.69
		CO	−1.68
Ni-GDY [168]	DFT	O <sub>2</sub> + CO	−1.09
		O	−3.21
		CO <sub>2</sub>	−0.08
		O <sub>2</sub>	−0.79
		CO	−1.25
Cu-GDY [168]	DFT	O <sub>2</sub> + CO	−1.43
		O	−3.21
		CO <sub>2</sub>	−0.37
Sc-GDY [165]			−2.59
Ti-GDY [165]	DFT	HCHO	−2.24
TM-GDY [161] TM = Ti, Sc, Li, Na, K, Ca	DFT (GGA)		[−0.197, −0.10]
	DFT (vdW-DF)	8H <sub>2</sub>	[−0.77, −0.194]
	DFT (DFT-D3)		[−0.345, −0.173]
Mo-GDY [163]	DFT	N <sub>2</sub>	[−1.35, −0.93]
TM-GDY [82] TM = Sc, Ti, V, Cr, Mn, Fe, Co, Ni, Cu, Y, Zr, Rh, Pd, Ag, La, Hf, Pt	DFT	N <sub>2</sub>	[−1.8, +0.12]
TM-GDY [160] TM = Cr, Mn, Fe, Co	DFT-D3	O <sub>2</sub>	[−2.52, −1.21]
		CO	[−1.57, −1.25]
TM-1N-GDY [160] TM = Cr, Mn, Fe, Co	DFT-D3	O <sub>2</sub>	[−2.56, −1.07]
		CO	[−1.78, −1.21]
TM-2N-GDY [160] TM = Cr, Mn, Fe, Co	DFT-D3	O <sub>2</sub>	[−2.31, −1.17]
		CO	[−1.94, −1.39]
Ru-GDY [162]	Experimental	H <sub>2</sub> O	Not reported
Fe-GDY [167]	DFT-D3/AIMD	CO <sub>2</sub>	Not reported

### 3.6. Hybrid Systems Doped with Transition Metals

Several studies have also focused on the TM-doping of hybrid carbon nanostructures starting. The most convenient places to dope a buckybowll have been studied by computational means, covering the binding possibilities of the transition-metal ion Cu<sup>+</sup>, and cations as Li<sup>+</sup>, Na<sup>+</sup>, K<sup>+</sup>, to buckybowlls on convenient locations where the gradient electron density favors the adsorption [169]. In other studies, authors have investigated the catalytic effect of Ni, Fe, and a Fe-Ni alloy on synthesizing metal-containing carbon nano-onions (CNOs) and studied their electrochemical hydrogen storage properties. They found that the electrochemical hydrogen storage capacity of the CNOs is in the order of Ni@CNOs > Fe<sub>0.64</sub>Ni<sub>0.36</sub>@CNOs > Fe<sub>3</sub>C@CNOs. The Ni@CNOs have a maximum hydrogen storage capacity of 1.42%. Large amounts of defects, good electrical conductivity, and electrocatalytic activity of the Ni particles are responsible for their excellent electrochemical performance [170].

In [171], the authors considered the doping of a semi-fullerene C<sub>30</sub> with titanium to adsorb molecules of CO and CO<sub>2</sub>. With an exploration involving density functional theory (DFT) and first-principles molecular dynamics (FPMD) at 300 K and atmospheric pressure, they found that the most stable adsorption of the titanium atom on C<sub>30</sub> occurs on the concave surface of the molecule. Besides, the considered molecules are chemisorbed, with no dissociation. The adsorption energies depend on the initial orientation of the

molecules concerning  $\text{TiC}_{30}$ . Similarly, in [172], density functional theory (DFT) was also used to study the adsorption of an  $\text{H}_2$  molecule in a system formed by a graphene layer and a Ti-doped semi-fullerene. The authors found that the semi-fullerene is bound to the graphene layer, with one of the hexagonal faces of the former being oriented into the latter. Besides, the semi-fullerene chemisorbs the titanium atom. Finally, the authors studied the interaction between the hydrogen molecule and the combined system, finding that the system can adsorb the  $\text{H}_2$  molecule. Table 11 shows the main quantitative results of this section.

**Table 11.** Summary of adsorption energies  $E_{\text{ads}}$  (in eV) for different TM-metallic doped hybrid systems and adsorbates. The type of study is also specified.

System	Type of Study	Adsorbate	$E_{\text{ads}}$
Ti- $\text{C}_{30}$ [171]	DFT	CO	[−0.897, −1.673]
		CO <sub>2</sub>	[−1.605, −1.247]
Ti-G-Semifullerene [172]	DFT	H <sub>2</sub>	−1.41
Ni-, Fe-CNOs [170]	Experimental	H <sub>2</sub>	Not reported

#### 4. Conclusions

We aimed to present the most important and recent advances in the study of polluting gas adsorption employing carbon nanostructures. The porous nature of the latter has made them a natural choice for developing sensing devices throughout the years, and physical features like diameter, curvature or size, influence their adsorption capabilities. The carbon nanostructures reviewed in general physically adsorb many of the pollutant gas molecules considered, and the interaction can usually increase by different means of nonmetal functionalizations or doping. However, transition-metal doping and decoration give better results overall, increasing their sensing properties, involving chemisorption in most cases studied. There have also been many systems showing a good adsorption–desorption cyclic performance, which makes them good candidates for sensing devices.

Among the transition metals used as dopants in the reviewed works, we found Ag, Au, Pt, Pd, Fe, Rh, Zr, Mo, Ti, Mn, Co, Ni, Cu, Sc, and V. Besides, we found the non-transition metals as dopants too: Zn, Si, P, S, As, Se, Te, Li, N, and B.

On the other hand, among the pollutant molecules investigated for adsorption in carbon nanostructures that we found in this review, we have  $\text{NO}_2$ ,  $\text{NH}_3$ ,  $\text{NH}_2$ ,  $\text{SO}_2$ ,  $\text{H}_2\text{S}$ ,  $\text{C}_2\text{H}_6\text{O}$ ,  $\text{C}_3\text{H}_6\text{O}$ ,  $\text{C}_7\text{H}_8$ ,  $\text{NO}$ ,  $\text{Cl}_2$ ,  $\text{CH}_4$ ,  $\text{N}_2\text{O}$ ,  $\text{CO}$ ,  $\text{C}_2\text{H}_4$ ,  $\text{CO}_2$ ,  $\text{O}_3$ ,  $\text{CH}_3\text{OH}$ ,  $\text{H}_2\text{CO}$ ,  $\text{H}_2\text{CO}_2$ ,  $\text{C}_2\text{H}_2$ ,  $\text{SF}_6$ ,  $\text{C}_2\text{N}_2$ ,  $\text{C}_6\text{H}_{14}$ ,  $\text{C}_7\text{H}_8$ ,  $\text{C}_2\text{H}_3\text{N}$ ,  $\text{CH}_2\text{Cl}_2$ ,  $\text{CH}_3\text{COOC}_2\text{H}_5$ ,  $(\text{CH}_3)_2\text{NH}$ ,  $\text{C}_3\text{H}_9\text{N}$ ,  $\text{AsH}_3$ . Moreover, the anticancer drugs 5-fluorouracil and temozolomide. We also found amphetamines. Finally, we also found the chemical warfare agents (CWAs) tabun, sarin, soman, cyclosarin, phosgene, and Lewisite molecules.

Carbon nanotubes and graphene are probably the most investigated systems, as shown by the abundance of cites. However, the detailed study of its adsorption properties is ongoing.

To end, we should mention that the study of the adsorption properties of carbon nanostructures is far from being completed. Relatively recent structures like graphdiyne have plenty of potential applications waiting for the investigation, and the building of hybrid systems has much to offer for materials scientists in the future.

**Author Contributions:** Conceptualization, L.F.M.; writing—original draft preparation, L.F.M., J.M.R.-d.-A. and M.C.; writing—review and editing, L.F.M. and J.M.R.-d.-A.; graphic materials, M.C.; funding acquisitions, L.F.M. All authors have read and agreed to the published version of the manuscript.

**Funding:** We thank Dirección General de Asuntos del Personal Académico de la Universidad Nacional Autónoma de México, partial financial support by Grant IN113220.

**Institutional Review Board Statement:** Not applicable.

**Informed Consent Statement:** Not applicable.

**Data Availability Statement:** Not applicable.

**Acknowledgments:** We thank Dirección General de Asuntos del Personal Académico de la Universidad Nacional Autónoma de México, partial financial support by Grant IN113220. We also appreciate UNAM-Miztli-Super-Computing Center technical assistance by the project LANCAD-UNAM-DGTIC-030.

**Conflicts of Interest:** The authors declare no conflict of interest.

## References

1. Kroto, H.W.; Heath, J.R.; O'Brien, S.C.; Curl, R.F.; Smalley, R.E. C<sub>60</sub>: Buckminsterfullerene. *Nature* **1985**, *318*, 162–163. [[CrossRef](#)]
2. Nasibulin, A.G.; Pikhitsa, P.V.; Jiang, H.; Brown, D.P.; Krasheninnikov, A.V.; Anisimov, A.S.; Queipo, P.; Moisala, A.; Gonzalez, D.; Lientschnig, G.; et al. A Novel Hybrid Carbon Material. *Nat. Nanotechnol.* **2007**, *2*, 156–161. [[CrossRef](#)] [[PubMed](#)]
3. Moisala, A.; Nasibulin, A.G.; Shandakov, S.D.; Jiang, H.; Kauppinen, E.I. On-Line Detection of Single-Walled Carbon Nanotube Formation during Aerosol Synthesis Methods. *Carbon* **2005**, *43*, 2066–2074. [[CrossRef](#)]
4. Delgado, J.L.; Herranz, M.; Martín, N. The Nano-Forms of Carbon. *J. Mater. Chem.* **2008**, *18*, 1417. [[CrossRef](#)]
5. Falcao, E.H.; Wudl, F. Carbon Allotropes: Beyond Graphite and Diamond. *J. Chem. Technol. Biotechnol.* **2007**, *82*, 524–531. [[CrossRef](#)]
6. Langenhorst, F.; Campione, M. Ideal and Real Structures of Different Forms of Carbon, with Some Remarks on Their Geological Significance. *J. Geol. Soc.* **2019**, *176*, 337–347. [[CrossRef](#)]
7. Pacheco, M.; Pacheco, J.; Valdivia, R.; Santana, A.; Tu, X.; Mendoza, D.; Frias, H.; Medina, L.; Macias, J. Green Applications of Carbon Nanostructures Produced by Plasma Techniques. *MRS Adv.* **2017**, *2*, 2647–2659. [[CrossRef](#)]
8. Lejaeghere, K.; Van Speybroeck, V.; Van Oost, G.; Cottenier, S. Error Estimates for Solid-State Density-Functional Theory Predictions: An Overview by Means of the Ground-State Elemental Crystals. *Crit. Rev. Solid State Mater. Sci.* **2014**, *39*, 1–24. [[CrossRef](#)]
9. Boyd, A.; Dube, I.; Fedorov, G.; Paranjape, M.; Barbara, P. Gas Sensing Mechanism of Carbon Nanotubes: From Single Tubes to High-Density Networks. *Carbon* **2014**, *69*, 417–423. [[CrossRef](#)]
10. Zhao, J.; Buldum, A.; Han, J.; Lu, J.P. Gas Molecule Adsorption in Carbon Nanotubes and Nanotube Bundles. *Nanotechnology* **2002**, *13*, 195–200. [[CrossRef](#)]
11. Feng, Y.; Wang, J.; Liu, Y.; Zheng, Q. Adsorption Equilibrium of Hydrogen Adsorption on Activated Carbon, Multi-Walled Carbon Nanotubes and Graphene Sheets. *Cryogenics* **2019**, *101*, 36–42. [[CrossRef](#)]
12. Panella, B.; Hirscher, M.; Roth, S. Hydrogen Adsorption in Different Carbon Nanostructures. *Carbon* **2005**, *43*, 2209–2214. [[CrossRef](#)]
13. Dhall, S.; Jaggi, N.; Nathawat, R. Functionalized Multiwalled Carbon Nanotubes Based Hydrogen Gas Sensor. *Sens. Actuators A Phys.* **2013**, *201*, 321–327. [[CrossRef](#)]
14. Elyassi, M.; Rashidi, A.; Hantehzadeh, M.R.; Elahi, S.M. Hydrogen Storage Behaviors by Adsorption on Multi-Walled Carbon Nanotubes. *J. Inorg. Organomet. Polym.* **2017**, *27*, 285–295. [[CrossRef](#)]
15. Lithoxoos, G.P.; Labropoulos, A.; Peristeras, L.D.; Kanellopoulos, N.; Samios, J.; Economou, I.G. Adsorption of N<sub>2</sub>, CH<sub>4</sub>, CO and CO<sub>2</sub> Gases in Single Walled Carbon Nanotubes: A Combined Experimental and Monte Carlo Molecular Simulation Study. *J. Supercrit. Fluids* **2010**, *55*, 510–523. [[CrossRef](#)]
16. Su, F.; Lu, C.; Cnen, W.; Bai, H.; Hwang, J.F. Capture of CO<sub>2</sub> from Flue Gas via Multiwalled Carbon Nanotubes. *Sci. Total Environ.* **2009**, *407*, 3017–3023. [[CrossRef](#)] [[PubMed](#)]
17. Hsu, S.-C.; Lu, C.; Su, F.; Zeng, W.; Chen, W. Thermodynamics and Regeneration Studies of CO<sub>2</sub> Adsorption on Multiwalled Carbon Nanotubes. *Chem. Eng. Sci.* **2010**, *65*, 1354–1361. [[CrossRef](#)]
18. Su, F.; Lu, C.; Chung, A.-J.; Liao, C.-H. CO<sub>2</sub> Capture with Amine-Loaded Carbon Nanotubes via a Dual-Column Temperature/Vacuum Swing Adsorption. *Appl. Energy* **2014**, *113*, 706–712. [[CrossRef](#)]
19. Inoue, S.; Tomita, Y.; Kokabu, T.; Matsumura, Y. Principles of Detection Mechanism for Adsorbed Gases Using Carbon Nanotube Nanomat. *Chem. Phys. Lett.* **2018**, *709*, 77–81. [[CrossRef](#)]
20. Fatemi, S.; Vesali-Naseh, M.; Cyrus, M.; Hashemi, J. Improving CO<sub>2</sub>/CH<sub>4</sub> Adsorptive Selectivity of Carbon Nanotubes by Functionalization with Nitrogen-Containing Groups. *Chem. Eng. Res. Des.* **2011**, *89*, 1669–1675. [[CrossRef](#)]
21. Lin, C.-C.; Gupta, S.; Chang, C.; Lee, C.-Y.; Tai, N.-H. Polyethylenimine-Polyethylene Glycol/Multi-Walled Carbon Nanotubes Bilayer Structure for Carbon Dioxide Gas Sensing at Room Temperature. *Mater. Lett.* **2021**, *297*, 129941. [[CrossRef](#)]
22. Rahimi, K.; Riahi, S.; Abbasi, M.; Fakhroueian, Z. Modification of Multi-Walled Carbon Nanotubes by 1,3-Diaminopropane to Increase CO<sub>2</sub> Adsorption Capacity. *J. Environ. Manag.* **2019**, *242*, 81–89. [[CrossRef](#)]
23. Faginas-Lago, N.; Apriliyanto, Y.B.; Lombardi, A. Confinement of CO<sub>2</sub> inside Carbon Nanotubes. *Eur. Phys. J. D* **2021**, *75*, 161. [[CrossRef](#)]
24. Mukhtar, A.; Mellon, N.; Saqib, S.; Khawar, A.; Rafiq, S.; Ullah, S.; Al-Sehemi, A.G.; Babar, M.; Bustam, M.A.; Khan, W.A.; et al. CO<sub>2</sub>/CH<sub>4</sub> Adsorption over Functionalized Multi-Walled Carbon Nanotubes; an Experimental Study, Isotherms Analysis, Mechanism, and Thermodynamics. *Microporous Mesoporous Mater.* **2020**, *294*, 109883. [[CrossRef](#)]

25. Delavar, M.; Asghar Ghoreyshi, A.; Jahanshahi, M.; Khalili, S.; Nabian, N. Equilibria and Kinetics of Natural Gas Adsorption on Multi-Walled Carbon Nanotube Material. *RSC Adv.* **2012**, *2*, 4490. [[CrossRef](#)]
26. Babu, D.J.; Lange, M.; Cherkashinin, G.; Issanin, A.; Staudt, R.; Schneider, J.J. Gas Adsorption Studies of CO<sub>2</sub> and N<sub>2</sub> in Spatially Aligned Double-Walled Carbon Nanotube Arrays. *Carbon* **2013**, *61*, 616–623. [[CrossRef](#)]
27. Liu, L.; Nicholson, D.; Bhatia, S.K. Impact of H<sub>2</sub>O on CO<sub>2</sub> Separation from Natural Gas: Comparison of Carbon Nanotubes and Disordered Carbon. *J. Phys. Chem. C* **2015**, *119*, 407–419. [[CrossRef](#)]
28. Chiang, Y.-C.; Wu, P.-Y. Adsorption Equilibrium of Sulfur Hexafluoride on Multi-Walled Carbon Nanotubes. *J. Hazard. Mater.* **2010**, *178*, 729–738. [[CrossRef](#)]
29. Lide, D.R. (Ed.) *CRC Handbook of Chemistry and Physics: A Ready-Reference Book of Chemical and Physical Data*, 81st ed.; CRC Press: Boca Raton, FL, USA, 2000; ISBN 978-0-8493-0481-1.
30. Kazachkin, D.V.; Nishimura, Y.; Irle, S.; Feng, X.; Vidic, R.; Borguet, E. Temperature and Pressure Dependence of Molecular Adsorption on Single Wall Carbon Nanotubes and the Existence of an “Adsorption/Desorption Pressure Gap”. *Carbon* **2010**, *48*, 1867–1875. [[CrossRef](#)]
31. Young, S.-J.; Lin, Z.-D. Ethanol Gas Sensors Composed of Carbon Nanotubes with Au Nanoparticles Adsorbed onto a Flexible PI Substrate. *ECS J. Solid State Sci. Technol.* **2017**, *6*, M130–M132. [[CrossRef](#)]
32. Abdulla, S.; Mathew, T.L.; Pullithadathil, B. Highly Sensitive, Room Temperature Gas Sensor Based on Polyaniline-Multiwalled Carbon Nanotubes (PANI/MWCNTs) Nanocomposite for Trace-Level Ammonia Detection. *Sens. Actuators B Chem.* **2015**, *221*, 1523–1534. [[CrossRef](#)]
33. Battie, Y.; Ducloux, O.; Thobois, P.; Dorval, N.; Lauret, J.S.; Attal-Trétout, B.; Loiseau, A. Gas Sensors Based on Thick Films of Semi-Conducting Single Walled Carbon Nanotubes. *Carbon* **2011**, *49*, 3544–3552. [[CrossRef](#)]
34. Chen, G.; Paronyan, T.M.; Pigos, E.M.; Harutyunyan, A.R. Enhanced Gas Sensing in Pristine Carbon Nanotubes under Continuous Ultraviolet Light Illumination. *Sci. Rep.* **2012**, *2*, 343. [[CrossRef](#)]
35. Huyen, D.N.; Tung, N.T.; Vinh, T.D.; Thien, N.D. Synergistic Effects in the Gas Sensitivity of Polypyrrole/Single Wall Carbon Nanotube Composites. *Sensors* **2012**, *12*, 7965–7974. [[CrossRef](#)] [[PubMed](#)]
36. Kuznetsova, A.; Yates, J.T.; Simonyan, V.V.; Johnson, J.K.; Huffman, C.B.; Smalley, R.E. Optimization of Xe Adsorption Kinetics in Single Walled Carbon Nanotubes. *J. Chem. Phys.* **2001**, *115*, 6691–6698. [[CrossRef](#)]
37. Beheshtian, J.; Peyghan, A.A.; Bagheri, Z. Nitrate Adsorption by Carbon Nanotubes in the Vacuum and Aqueous Phase. *Mon. Chem.* **2012**, *143*, 1623–1626. [[CrossRef](#)]
38. Beheshtian, J.; Peyghan, A.A.; Bagheri, Z. Formaldehyde Adsorption on the Interior and Exterior Surfaces of CN Nanotubes. *Struct. Chem.* **2013**, *24*, 1331–1337. [[CrossRef](#)]
39. Hu, Z.; Xie, H.; Wang, Q.; Chen, S. Adsorption and Diffusion of Sulfur Dioxide and Nitrogen in Single-Wall Carbon Nanotubes. *J. Mol. Graph. Model.* **2019**, *88*, 62–70. [[CrossRef](#)] [[PubMed](#)]
40. Li, M.; Wu, S.C.; Shih, Y. Characterization of Volatile Organic Compound Adsorption on Multiwall Carbon Nanotubes under Different Levels of Relative Humidity Using Linear Solvation Energy Relationship. *J. Hazard. Mater.* **2016**, *315*, 35–41. [[CrossRef](#)]
41. Wang, Y.; Yeow, J.T.W. A Review of Carbon Nanotubes-Based Gas Sensors. *J. Sens.* **2009**, *2009*, 493904. [[CrossRef](#)]
42. Casolo, S.; Løvvik, O.M.; Martinazzo, R.; Tantardini, G.F. Understanding Adsorption of Hydrogen Atoms on Graphene. *J. Chem. Phys.* **2009**, *130*, 054704. [[CrossRef](#)]
43. Feijó, T.O.; Rolim, G.K.; Corrêa, S.A.; Radtke, C.; Soares, G.V. Thermally Driven Hydrogen Interaction with Single-Layer Graphene on SiO<sub>2</sub>/Si Substrates Quantified by Isotopic Labeling. *J. Appl. Phys.* **2020**, *128*, 225702. [[CrossRef](#)]
44. Sunnardianto, G.K.; Bokas, G.; Hussein, A.; Walters, C.; Moulτος, O.A.; Dey, P. Efficient Hydrogen Storage in Defective Graphene and Its Mechanical Stability: A Combined Density Functional Theory and Molecular Dynamics Simulation Study. *Int. J. Hydrog. Energy* **2021**, *46*, 5485–5494. [[CrossRef](#)]
45. Leenaerts, O.; Partoens, B.; Peeters, F.M. Adsorption of H<sub>2</sub>O, NH<sub>3</sub>, CO, NO<sub>2</sub>, and NO on Graphene: A First-Principles Study. *Phys. Rev. B* **2008**, *77*, 125416. [[CrossRef](#)]
46. Bo, Z.; Guo, X.; Wei, X.; Yang, H.; Yan, J.; Cen, K. Density Functional Theory Calculations of NO<sub>2</sub> and H<sub>2</sub>S Adsorption on the Group 10 Transition Metal (Ni, Pd and Pt) Decorated Graphene. *Phys. E Low-Dimens. Syst. Nanostruct.* **2019**, *109*, 156–163. [[CrossRef](#)]
47. Gao, H.; Liu, Z. DFT Study of NO Adsorption on Pristine Graphene. *RSC Adv.* **2017**, *7*, 13082–13091. [[CrossRef](#)]
48. Gao, X.; Zhou, Q.; Wang, J.; Xu, L.; Zeng, W. Performance of Intrinsic and Modified Graphene for the Adsorption of H<sub>2</sub>S and CH<sub>4</sub>: A DFT Study. *Nanomaterials* **2020**, *10*, 299. [[CrossRef](#)]
49. Huang, S.; Panes-Ruiz, L.A.; Croy, A.; Löffler, M.; Khavrus, V.; Bezugly, V.; Cuniberti, G. Highly Sensitive Room Temperature Ammonia Gas Sensor Using Pristine Graphene: The Role of Biocompatible Stabilizer. *Carbon* **2021**, *173*, 262–270. [[CrossRef](#)]
50. Lazar, P.; Karlický, F.; Jurečka, P.; Kocman, M.; Otyepková, E.; Šafařová, K.; Otyepka, M. Adsorption of Small Organic Molecules on Graphene. *J. Am. Chem. Soc.* **2013**, *135*, 6372–6377. [[CrossRef](#)]
51. Salih, E.; Ayesh, A.I. Co-Doped Zigzag Graphene Nanoribbon Based Gas Sensor for Sensitive Detection of H<sub>2</sub>S: DFT Study. *Superlattices Microstruct.* **2021**, *155*, 106900. [[CrossRef](#)]
52. Karami, Z.; Hamed Mashhadzadeh, A.; Habibzadeh, S.; Ganjali, M.R.; Ghardi, E.M.; Hasnaoui, A.; Vatanpour, V.; Sharma, G.; Esmaeili, A.; Stadler, F.J.; et al. Atomic Simulation of Adsorption of SO<sub>2</sub> Pollutant by Metal (Zn, Be)-Oxide and Ni-Decorated Graphene: A First-Principles Study. *J. Mol. Model.* **2021**, *27*, 70. [[CrossRef](#)] [[PubMed](#)]

53. Xie, Y.; Cao, S.; Wu, X.; Yu, B.-Y.; Chen, L.-Y.; Zhang, J.-M. Density Functional Theory Study of Hydrogen Sulfide Adsorption onto Transition Metal-Doped Bilayer Graphene Using External Electric Fields. *Phys. E Low-Dimens. Syst. Nanostruct.* **2020**, *124*, 114252. [[CrossRef](#)]
54. Gui, Y.; Peng, X.; Liu, K.; Ding, Z. Adsorption of C<sub>2</sub>H<sub>2</sub>, CH<sub>4</sub> and CO on Mn-Doped Graphene: Atomic, Electronic, and Gas-Sensing Properties. *Phys. E Low-Dimens. Syst. Nanostruct.* **2020**, *119*, 113959. [[CrossRef](#)]
55. Shukri, M.S.M.; Saimin, M.N.S.; Yaakob, M.K.; Yahya, M.Z.A.; Taib, M.F.M. Structural and Electronic Properties of CO and NO Gas Molecules on Pd-Doped Vacancy Graphene: A First Principles Study. *Appl. Surf. Sci.* **2019**, *494*, 817–828. [[CrossRef](#)]
56. Jia, X.; An, L. The Adsorption of Nitrogen Oxides on Noble Metal-Doped Graphene: The First-Principles Study. *Mod. Phys. Lett. B* **2019**, *33*, 1950044. [[CrossRef](#)]
57. Li, Y.; Sun, X.; Zhou, L.; Ning, P.; Tang, L. Density Functional Theory Analysis of Selective Adsorption of AsH<sub>3</sub> on Transition Metal-Doped Graphene. *J. Mol. Model.* **2019**, *25*, 145. [[CrossRef](#)]
58. Khodadadi, Z. Evaluation of H<sub>2</sub>S Sensing Characteristics of Metals-Doped Graphene and Metals-Decorated Graphene: Insights from DFT Study. *Phys. E Low-Dimens. Syst. Nanostruct.* **2018**, *99*, 261–268. [[CrossRef](#)]
59. Zhang, T.; Sun, H.; Wang, F.; Zhang, W.; Tang, S.; Ma, J.; Gong, H.; Zhang, J. Adsorption of Phosgene Molecule on the Transition Metal-Doped Graphene: First Principles Calculations. *Appl. Surf. Sci.* **2017**, *425*, 340–350. [[CrossRef](#)]
60. Promthong, N.; Tabtimsai, C.; Rakrai, W.; Wannoo, B. Transition Metal-Doped Graphene Nanoflakes for CO and CO<sub>2</sub> Storage and Sensing Applications: A DFT Study. *Struct. Chem.* **2020**, *31*, 2237–2247. [[CrossRef](#)]
61. Chuvilin, A.; Kaiser, U.; Bichoutskaia, E.; Besley, N.A.; Khlobystov, A.N. Direct Transformation of Graphene to Fullerene. *Nat. Chem.* **2010**, *2*, 450–453. [[CrossRef](#)]
62. Manna, A.K.; Pati, S.K. Stability and Electronic Structure of Carbon Capsules with Superior Gas Storage Properties: A Theoretical Study. *Chem. Phys.* **2013**, *426*, 23–30. [[CrossRef](#)]
63. Khan, A.A.; Ahmad, I.; Ahmad, R. Influence of Electric Field on CO<sub>2</sub> Removal by P-Doped C<sub>60</sub>-Fullerene: A DFT Study. *Chem. Phys. Lett.* **2020**, *742*, 137155. [[CrossRef](#)]
64. Tascón, J.M.D.; Bottani, E.J. Ethylene Physisorption on C<sub>60</sub> Fullerene. *Carbon* **2004**, *42*, 1333–1337. [[CrossRef](#)]
65. Furuuchi, N.; Shrestha, R.; Yamashita, Y.; Hirao, T.; Ariga, K.; Shrestha, L. Self-Assembled Fullerene Crystals as Excellent Aromatic Vapor Sensors. *Sensors* **2019**, *19*, 267. [[CrossRef](#)]
66. Khan, A.A.; Ahmad, R.; Ahmad, I. Removal of Nitrous and Carbon Mono Oxide from Flue Gases by Si-Coordinated Nitrogen Doped C<sub>60</sub>-Fullerene: A DFT Approach. *Mol. Catal.* **2021**, *509*, 111674. [[CrossRef](#)]
67. Haghgoo, S.; Nekoei, A.-R. Metal Oxide Adsorption on Fullerene C<sub>60</sub> and Its Potential for Adsorption of Pollutant Gases; Density Functional Theory Studies. *RSC Adv.* **2021**, *11*, 17377–17390. [[CrossRef](#)]
68. Bubenchikov, M.A.; Bubenchikov, A.M.; Usenko, O.V.; Tsyrenova, V.B.; Budaev, S.O. Ability of Fullerene to Accumulate Hydrogen. *EPJ Web Conf.* **2016**, *110*, 01077. [[CrossRef](#)]
69. Saha, D.; Deng, S. Hydrogen Adsorption on Partially Truncated and Open Cage C<sub>60</sub> Fullerene. *Carbon* **2010**, *48*, 3471–3476. [[CrossRef](#)]
70. Kaiser, A.; Leidlmair, C.; Bartl, P.; Zöttl, S.; Denifl, S.; Mauracher, A.; Probst, M.; Scheier, P.; Echt, O. Adsorption of Hydrogen on Neutral and Charged Fullerene: Experiment and Theory. *J. Chem. Phys.* **2013**, *138*, 074311. [[CrossRef](#)]
71. Kalateh, K.; Cordshooli, G.A.; Kheirollahpoor, S. Hydrogen Adsorption, Structural, Electronic, and Spectroscopic Properties of C<sub>32</sub>, B<sub>16</sub>N<sub>16</sub>, and B<sub>8</sub>C<sub>24</sub> by DFT Calculations. *Fuller. Nanotub. Carbon Nanostruct.* **2017**, *25*, 459–465. [[CrossRef](#)]
72. Barajas-Barraza, R.E.; Guirado-López, R.A. Endohedral Nitrogen Storage in Carbon Fullerene Structures: Physisorption to Chemisorption Transition with Increasing Gas Pressure. *J. Chem. Phys.* **2009**, *130*, 234706. [[CrossRef](#)]
73. Esrafil, M.D.; Janebi, H. B-, N-Doped and BN Codoped C<sub>60</sub> Heterofullerenes for Environmental Monitoring of NO and NO<sub>2</sub>: A DFT Study. *Mol. Phys.* **2020**, *118*, e1631495. [[CrossRef](#)]
74. Acosta-Gutiérrez, S.; Bretón, J.; Llorente, J.M.G.; Hernández-Rojas, J. Optimal Covering of C<sub>60</sub> Fullerene by Rare Gases. *J. Chem. Phys.* **2012**, *137*, 074306. [[CrossRef](#)]
75. Siadati, S.A.; Vessally, E.; Hosseinian, A.; Edjlali, L. Possibility of Sensing, Adsorbing, and Destructing the Tabun-2D-Skeletal (Tabun Nerve Agent) by C<sub>20</sub> Fullerene and Its Boron and Nitrogen Doped Derivatives. *Synth. Met.* **2016**, *220*, 606–611. [[CrossRef](#)]
76. Najafi, M. Density Functional Study of Cyanogen (C<sub>2</sub>N<sub>2</sub>) Sensing Using OH Functionalized Fullerene (C<sub>60</sub>) and Germanium-Fullerene (Ge<sub>60</sub>). *Vacuum* **2016**, *134*, 88–91. [[CrossRef](#)]
77. Bashiri, S.; Vessally, E.; Bekhradnia, A.; Hosseinian, A.; Edjlali, L. Utility of Extrinsic [60] Fullerenes as Work Function Type Sensors for Amphetamine Drug Detection: DFT Studies. *Vacuum* **2017**, *136*, 156–162. [[CrossRef](#)]
78. Ellessawy, N.A.; El-Sayed, E.M.; Ali, S.; Elkady, M.F.; Elnouby, M.; Hamad, H.A. One-Pot Green Synthesis of Magnetic Fullerene Nanocomposite for Adsorption Characteristics. *J. Water Process Eng.* **2020**, *34*, 101047. [[CrossRef](#)]
79. El Mahdy, A.M. Density Functional Investigation of CO and NO Adsorption on TM-Decorated C<sub>60</sub> Fullerene. *Appl. Surf. Sci.* **2016**, *383*, 353–366. [[CrossRef](#)]
80. Khan, A.A.; Ahmad, R.; Ahmad, I.; Su, X. Selective Adsorption of CO<sub>2</sub> from Gas Mixture by P-Decorated C<sub>24</sub>N<sub>24</sub> Fullerene Assisted by an Electric Field: A DFT Approach. *J. Mol. Graph. Model.* **2021**, *103*, 107806. [[CrossRef](#)]
81. Wu, P.; Du, P.; Zhang, H.; Cai, C. Graphdiyne as a Metal-Free Catalyst for Low-Temperature CO Oxidation. *Phys. Chem. Chem. Phys.* **2014**, *16*, 5640–5648. [[CrossRef](#)] [[PubMed](#)]

82. Feng, Z.; Tang, Y.; Chen, W.; Li, Y.; Li, R.; Ma, Y.; Dai, X. Graphdiyne Coordinated Transition Metals as Single-Atom Catalysts for Nitrogen Fixation. *Phys. Chem. Chem. Phys.* **2020**, *22*, 9216–9224. [[CrossRef](#)]
83. Ebadi, M.; Reisi-Vanani, A. Methanol and Carbon Monoxide Sensing and Capturing by Pristine and Ca-Decorated Graphdiyne: A DFT-D2 Study. *Phys. E Low-Dimens. Syst. Nanostruct.* **2021**, *125*, 114425. [[CrossRef](#)]
84. Yang, Z.; Zhang, Y.; Guo, M.; Yun, J. Adsorption of Hydrogen and Oxygen on Graphdiyne and Its BN Analog Sheets: A Density Functional Theory Study. *Comput. Mater. Sci.* **2019**, *160*, 197–206. [[CrossRef](#)]
85. Chen, X.; Gao, P.; Guo, L.; Zhang, S. Graphdiyne as a Promising Material for Detecting Amino Acids. *Sci. Rep.* **2015**, *5*, 16720. [[CrossRef](#)]
86. Nagarajan, V.; Srimathi, U.; Chandiramouli, R. First-Principles Insights on Detection of Dimethyl Amine and Trimethyl Amine Vapors Using Graphdiyne Nanosheets. *Comput. Theor. Chem.* **2018**, *1123*, 119–127. [[CrossRef](#)]
87. Srimathi, U.; Nagarajan, V.; Chandiramouli, R. Investigation on Graphdiyne Nanosheet in Adsorption of Sorafenib and Regorafenib Drugs: A DFT Approach. *J. Mol. Liq.* **2019**, *277*, 776–785. [[CrossRef](#)]
88. Nagarajan, V.; Chandiramouli, R. Investigation of NH<sub>3</sub> Adsorption Behavior on Graphdiyne Nanosheet and Nanotubes: A First-Principles Study. *J. Mol. Liq.* **2018**, *249*, 24–32. [[CrossRef](#)]
89. Bhuvaneshwari, R.; Princy Maria, J.; Nagarajan, V.; Chandiramouli, R. Graphdiyne Nanosheets as a Sensing Medium for Formaldehyde and Formic Acid—A First-Principles Outlook. *Comput. Theor. Chem.* **2020**, *1176*, 112751. [[CrossRef](#)]
90. Lv, Q.; Si, W.; He, J.; Sun, L.; Zhang, C.; Wang, N.; Yang, Z.; Li, X.; Wang, X.; Deng, W.; et al. Selectively Nitrogen-Doped Carbon Materials as Superior Metal-Free Catalysts for Oxygen Reduction. *Nat. Commun.* **2018**, *9*, 3376. [[CrossRef](#)]
91. Song, M.; Chen, Y.; Liu, X.; Xu, W.; Zhao, Y.; Zhang, M.; Zhang, C. A First-Principles Study of Gas Molecule Adsorption on Hydrogen-Substituted Graphdiyne. *Phys. Lett. A* **2020**, *384*, 126332. [[CrossRef](#)]
92. Xu, P.; Na, N.; Mohamadi, A. Investigation the Application of Pristine Graphdiyne (GDY) and Boron-Doped Graphdiyne (BGDY) as an Electronic Sensor for Detection of Anticancer Drug. *Comput. Theor. Chem.* **2020**, *1190*, 112996. [[CrossRef](#)]
93. Yuan, J.; Mohamadi, A. Study the Adsorption Process of 5-Fluorouracil Drug on the Pristine and Doped Graphdiyne Nanosheet. *J. Mol. Model.* **2021**, *27*, 32. [[CrossRef](#)]
94. Feng, Z.; Ma, Y.; Li, Y.; Li, R.; Tang, Y.; Dai, X. Oxygen Molecule Dissociation on Heteroatom Doped Graphdiyne. *Appl. Surf. Sci.* **2019**, *494*, 421–429. [[CrossRef](#)]
95. Rangel, E.; Ramirez-de-Arellano, J.M.; Magana, L.F. Variation of Hydrogen Adsorption with Increasing Li Doping on Carbon Nanotubes: Variation of Hydrogen Adsorption with Increasing Li Doping on CNTs. *Phys. Status Solidi B* **2011**, *248*, 1420–1424. [[CrossRef](#)]
96. Rangel, E.; Ramirez-Arellano, J.M.; Carrillo, I.; Magana, L.F. Hydrogen Adsorption around Lithium Atoms Anchored on Graphene Vacancies. *Int. J. Hydrog. Energy* **2011**, *36*, 13657–13662. [[CrossRef](#)]
97. Kim, J.; Kang, S.; Lim, J.; Kim, W.Y. Study of Li Adsorption on Graphdiyne Using Hybrid DFT Calculations. *ACS Appl. Mater. Interfaces* **2019**, *11*, 2677–2683. [[CrossRef](#)] [[PubMed](#)]
98. Feng, Z.; Su, G.; Ding, H.; Ma, Y.; Li, Y.; Tang, Y.; Dai, X. Atomic Alkali Metal Anchoring on Graphdiyne as Single-Atom Catalysts for Capture and Conversion of CO<sub>2</sub> to HCOOH. *Mol. Catal.* **2020**, *494*, 111142. [[CrossRef](#)]
99. Liu, T.; Wang, Q.; Wang, G.; Bao, X. Electrochemical CO<sub>2</sub> Reduction on Graphdiyne: A DFT Study. *Green Chem.* **2021**, *23*, 1212–1219. [[CrossRef](#)]
100. Feng, Z.; Tang, Y.; Ma, Y.; Li, Y.; Dai, Y.; Ding, H.; Su, G.; Dai, X. Theoretical Investigation of CO<sub>2</sub> Electroreduction on N (B)-Doped Graphdiyne Monolayer Supported Single Copper Atom. *Appl. Surf. Sci.* **2021**, *538*, 148145. [[CrossRef](#)]
101. Wu, Y.; Chen, X.; Weng, K.; Jiang, J.; Ong, W.; Zhang, P.; Zhao, X.; Li, N. Highly Sensitive and Selective Gas Sensor Using Heteroatom Doping Graphdiyne: A DFT Study. *Adv. Electron. Mater.* **2021**, *7*, 2001244. [[CrossRef](#)]
102. Cao, J.; Li, N.; Zeng, X. Exploring the Synergistic Effect of B–N Doped Defective Graphdiyne for N<sub>2</sub> Fixation. *New J. Chem.* **2021**, *45*, 6327–6335. [[CrossRef](#)]
103. Chen, X.; Lin, Z.-Z. Single-Layer Graphdiyne-Covered Pt(111) Surface: Improved Catalysis Confined under Two-Dimensional Overlayer. *J. Nanopart. Res.* **2018**, *20*, 136. [[CrossRef](#)]
104. Khan, S.; Yar, M.; Kosar, N.; Ayub, K.; Arshad, M.; Zahid, M.N.; Mahmood, T. First-Principles Study for Exploring the Adsorption Behavior of G-Series Nerve Agents on Graphdiyne Surface. *Comput. Theor. Chem.* **2020**, *1191*, 113043. [[CrossRef](#)]
105. Sajid, H.; Khan, S.; Ayub, K.; Mahmood, T. Effective Adsorption of A-Series Chemical Warfare Agents on Graphdiyne Nanoflake: A DFT Study. *J. Mol. Model.* **2021**, *27*, 117. [[CrossRef](#)] [[PubMed](#)]
106. Khan, S.; Sajid, H.; Ayub, K.; Mahmood, T. Sensing of Toxic Lewisite (L<sub>1</sub>, L<sub>2</sub>, and L<sub>3</sub>) Molecules by Graphdiyne Nanoflake Using Density Functional Theory Calculations and Quantum Theory of Atoms in Molecule Analysis. *J. Phys. Org. Chem.* **2021**, *34*, e4181. [[CrossRef](#)]
107. Mashhadzadeh, A.H.; Vahedi, A.M.; Ardjmand, M.; Ahangari, M.G. Investigation of Heavy Metal Atoms Adsorption onto Graphene and Graphdiyne Surface: A Density Functional Theory Study. *Superlattices Microstruct.* **2016**, *100*, 1094–1102. [[CrossRef](#)]
108. Seif, A.; López, M.J.; Granja-DelRío, A.; Azizi, K.; Alonso, J.A. Adsorption and Growth of Palladium Clusters on Graphdiyne. *Phys. Chem. Chem. Phys.* **2017**, *19*, 19094–19102. [[CrossRef](#)] [[PubMed](#)]
109. Wang, X.; Ma, C.; Chen, K.; Li, H.; Wang, P. Interaction between Nanobuds and Hydrogen Molecules: A First-Principles Study. *Phys. Lett. A* **2009**, *374*, 87–90. [[CrossRef](#)]



110. Wu, C.-D.; Fang, T.-H.; Lo, J.-Y. Effects of Pressure, Temperature, and Geometric Structure of Pillared Graphene on Hydrogen Storage Capacity. *Int. J. Hydrog. Energy* **2012**, *37*, 14211–14216. [[CrossRef](#)]
111. Hassani, A.; Hamed Mosavian, M.T.; Ahmadpour, A.; Farhadian, N. Hybrid Molecular Simulation of Methane Storage inside Pillared Graphene. *J. Chem. Phys.* **2015**, *142*, 234704. [[CrossRef](#)]
112. Baykasoglu, C.; Mert, H.; Deniz, C.U. Grand Canonical Monte Carlo Simulations of Methane Adsorption in Fullerene Pillared Graphene Nanocomposites. *J. Mol. Graph. Model.* **2021**, *106*, 107909. [[CrossRef](#)] [[PubMed](#)]
113. Ozturk, Z.; Baykasoglu, C.; Kirca, M. Sandwiched Graphene-Fullerene Composite: A Novel 3-D Nanostructured Material for Hydrogen Storage. *Int. J. Hydrog. Energy* **2016**, *41*, 6403–6411. [[CrossRef](#)]
114. Ugarte, D. Curling and Closure of Graphitic Networks under Electron-Beam Irradiation. *Nature* **1992**, *359*, 707–709. [[CrossRef](#)]
115. Goclon, J.; Bankiewicz, B.; Kolek, P.; Winkler, K. Role of Nitrogen Doping in Stoichiometric and Defective Carbon Nano-Onions: Structural Diversity from DFT Calculations. *Carbon* **2021**, *176*, 198–208. [[CrossRef](#)]
116. Hussain, M.A.; Vijay, D.; Sastry, G.N. Buckybowls as Adsorbents for CO<sub>2</sub>, CH<sub>4</sub>, and C<sub>2</sub>H<sub>2</sub>: Binding and Structural Insights from Computational Study. *J. Comput. Chem.* **2016**, *37*, 366–377. [[CrossRef](#)]
117. Zhang, C.; Li, J.; Liu, E.; He, C.; Shi, C.; Du, X.; Hauge, R.H.; Zhao, N. Synthesis of Hollow Carbon Nano-Onions and Their Use for Electrochemical Hydrogen Storage. *Carbon* **2012**, *50*, 3513–3521. [[CrossRef](#)]
118. Nikmaram, F.R.; Khoddamzadeh, A. Chemical Shielding of Doped Nitrogen on C<sub>20</sub> Cage and Bowl Fullerenes. *J. Struct. Chem.* **2017**, *58*, 173–177. [[CrossRef](#)]
119. Zhang, W.-D.; Zhang, W.-H. Carbon Nanotubes as Active Components for Gas Sensors. *J. Sens.* **2009**, *2009*, 160698. [[CrossRef](#)]
120. Kong, J.; Chapline, M.G.; Dai, H. Functionalized Carbon Nanotubes for Molecular Hydrogen Sensors. *Adv. Mater.* **2001**, *13*, 1384–1386. [[CrossRef](#)]
121. Sayago, I.; Terrado, E.; Aleixandre, M.; Horrillo, M.C.; Fernández, M.J.; Lozano, J.; Lafuente, E.; Maser, W.K.; Benito, A.M.; Martinez, M.T.; et al. Novel Selective Sensors Based on Carbon Nanotube Films for Hydrogen Detection. *Sens. Actuators B Chem.* **2007**, *122*, 75–80. [[CrossRef](#)]
122. Mubeen, S.; Zhang, T.; Yoo, B.; Deshusses, M.A.; Myung, N.V. Palladium Nanoparticles Decorated Single-Walled Carbon Nanotube Hydrogen Sensor. *J. Phys. Chem. C* **2007**, *111*, 6321–6327. [[CrossRef](#)]
123. Sun, Y.; Wang, H.H. Electrodeposition of Pd Nanoparticles on Single-Walled Carbon Nanotubes for Flexible Hydrogen Sensors. *Appl. Phys. Lett.* **2007**, *90*, 213107. [[CrossRef](#)]
124. Sippel-Oakley, J.; Wang, H.-T.; Kang, B.S.; Wu, Z.; Ren, F.; Rinzler, A.G.; Pearton, S.J. Carbon Nanotube Films for Room Temperature Hydrogen Sensing. *Nanotechnology* **2005**, *16*, 2218–2221. [[CrossRef](#)] [[PubMed](#)]
125. Ding, D.; Chen, Z.; Rajaputra, S.; Singh, V. Hydrogen Sensors Based on Aligned Carbon Nanotubes in an Anodic Aluminum Oxide Template with Palladium as a Top Electrode. *Sens. Actuators B Chem.* **2007**, *124*, 12–17. [[CrossRef](#)]
126. Lu, Y.; Li, J.; Han, J.; Ng, H.-T.; Binder, C.; Partridge, C.; Meyyappan, M. Room Temperature Methane Detection Using Palladium Loaded Single-Walled Carbon Nanotube Sensors. *Chem. Phys. Lett.* **2004**, *391*, 344–348. [[CrossRef](#)]
127. Li, Y.; Wang, H.; Chen, Y.; Yang, M. A Multi-Walled Carbon Nanotube/Palladium Nanocomposite Prepared by a Facile Method for the Detection of Methane at Room Temperature. *Sens. Actuators B Chem.* **2008**, *132*, 155–158. [[CrossRef](#)]
128. Kumar, M.K.; Ramaprabhu, S. Nanostructured Pt Functionalized Multiwalled Carbon Nanotube Based Hydrogen Sensor. *J. Phys. Chem. B* **2006**, *110*, 11291–11298. [[CrossRef](#)]
129. Krishnakumar, M.; Ramaprabhu, S. Palladium Dispersed Multiwalled Carbon Nanotube Based Hydrogen Sensor for Fuel Cell Applications. *Int. J. Hydrog. Energy* **2007**, *32*, 2518–2526. [[CrossRef](#)]
130. Krishna Kumar, M.; Leela Mohana Reddy, A.; Ramaprabhu, S. Exfoliated Single-Walled Carbon Nanotube-Based Hydrogen Sensor. *Sens. Actuators B Chem.* **2008**, *130*, 653–660. [[CrossRef](#)]
131. Kamarchuk, G.V.; Kolobov, I.G.; Khotkevich, A.V.; Yanson, I.K.; Pospelov, A.P.; Levitsky, I.A.; Euler, W.B. New Chemical Sensors Based on Point Heterocontact between Single Wall Carbon Nanotubes and Gold Wires. *Sens. Actuators B Chem.* **2008**, *134*, 1022–1026. [[CrossRef](#)]
132. Penza, M.; Cassano, G.; Rossi, R.; Alvisi, M.; Rizzo, A.; Signore, M.A.; Dikonimos, T.; Serra, E.; Giorgi, R. Enhancement of Sensitivity in Gas Chemiresistors Based on Carbon Nanotube Surface Functionalized with Noble Metal (Au, Pt) Nanoclusters. *Appl. Phys. Lett.* **2007**, *90*, 173123. [[CrossRef](#)]
133. Espinosa, E.H.; Ionescu, R.; Bittencourt, C.; Felten, A.; Erni, R.; Van Tendeloo, G.; Pireaux, J.-J.; Llobet, E. Metal-Decorated Multi-Wall Carbon Nanotubes for Low Temperature Gas Sensing. *Thin Solid Film.* **2007**, *515*, 8322–8327. [[CrossRef](#)]
134. Star, A.; Joshi, V.; Skarupo, S.; Thomas, D.; Gabriel, J.-C.P. Gas Sensor Array Based on Metal-Decorated Carbon Nanotubes. *J. Phys. Chem. B* **2006**, *110*, 21014–21020. [[CrossRef](#)] [[PubMed](#)]
135. Lu, Y.; Partridge, C.; Meyyappan, M.; Li, J. A Carbon Nanotube Sensor Array for Sensitive Gas Discrimination Using Principal Component Analysis. *J. Electroanal. Chem.* **2006**, *593*, 105–110. [[CrossRef](#)]
136. Kwon, Y.J.; Na, H.G.; Kang, S.Y.; Choi, S.-W.; Kim, S.S.; Kim, H.W. Selective Detection of Low Concentration Toluene Gas Using Pt-Decorated Carbon Nanotubes Sensors. *Sens. Actuators B Chem.* **2016**, *227*, 157–168. [[CrossRef](#)]
137. Tabtimsai, C.; Keawwangchai, S.; Nunthaboot, N.; Ruangpornvisuti, V.; Wannoo, B. Density Functional Investigation of Hydrogen Gas Adsorption on Fe-doped Pristine and Stone–Wales Defected Single-walled Carbon Nanotubes. *J. Mol. Model.* **2012**, *18*, 3941–3949. [[CrossRef](#)]

138. Rather, S. Hydrogen Uptake of Ti-Decorated Multiwalled Carbon Nanotube Composites. *Int. J. Hydrog. Energy* **2021**, *46*, 17793–17801. [[CrossRef](#)]
139. Dixit, S.; Patodia, T.; Sharma, K.B.; Katyayan, S.; Dixit, A.; Jain, S.K.; Agarwal, G.; Tripathi, B. Adsorption Characteristics of MWNTs via Intercalation of Nickel. *Mater. Today Proc.* **2021**, *38*, 1233–1236. [[CrossRef](#)]
140. Zhang, X.; Dai, Z.; Wei, L.; Liang, N.; Wu, X. Theoretical Calculation of the Gas-Sensing Properties of Pt-Decorated Carbon Nanotubes. *Sensors* **2013**, *13*, 15159–15171. [[CrossRef](#)]
141. Zhang, X.; Dai, Z.; Chen, Q.; Tang, J. A DFT Study of SO<sub>2</sub> and H<sub>2</sub>S Gas Adsorption on Au-Doped Single-Walled Carbon Nanotubes. *Phys. Scr.* **2014**, *89*, 065803. [[CrossRef](#)]
142. Lam, A.D.K.-T.; Lin, Z.-D.; Lu, H.-Y.; Young, S.-J. Carbon Nanotubes with Adsorbed Au Nanoparticles for Sensing Propanone Gas. *Microsyst. Technol.* **2019**, 1–4. [[CrossRef](#)]
143. Li, S.; Jiang, J. Adsorption Behavior Analyses of Several Small Gas Molecules onto Rh-Doped Single-Walled Carbon Nanotubes. *Appl. Phys. A* **2017**, *123*, 669. [[CrossRef](#)]
144. Kuganathan, N.; Chroneos, A. Ru-Doped Single Walled Carbon Nanotubes as Sensors for SO<sub>2</sub> and H<sub>2</sub>S Detection. *Chemosensors* **2021**, *9*, 120. [[CrossRef](#)]
145. Li, K.; Wang, W.; Cao, D. Metal (Pd, Pt)-Decorated Carbon Nanotubes for CO and NO Sensing. *Sens. Actuators B Chem.* **2011**, *159*, 171–177. [[CrossRef](#)]
146. Yoosefian, M. Powerful Greenhouse Gas Nitrous Oxide Adsorption onto Intrinsic and Pd Doped Single Walled Carbon Nanotube. *Appl. Surf. Sci.* **2017**, *392*, 225–230. [[CrossRef](#)]
147. Cui, H.; Zhang, X.; Yao, Q.; Miao, Y.; Tang, J. Rh-Doped Carbon Nanotubes as a Superior Media for the Adsorption of O<sub>2</sub> and O<sub>3</sub> Molecules: A Density Functional Theory Study. *Carbon Lett.* **2018**, *28*, 55–59. [[CrossRef](#)]
148. Young, S.J.; Lin, Z.D. Acetone Gas Sensors Composed of Carbon Nanotubes with Adsorbed Au Nanoparticles on Plastic Substrate. *Microsyst. Technol.* **2018**, *24*, 3973–3976. [[CrossRef](#)]
149. Pei, P.; Whitwick, M.B.; Kureshi, S.; Cannon, M.; Quan, G.; Kjeang, E. Hydrogen Storage Mechanism in Transition Metal Decorated Graphene Oxide: The Symbiotic Effect of Oxygen Groups and High Layer Spacing. *Int. J. Hydrog. Energy* **2020**, *45*, 6713–6726. [[CrossRef](#)]
150. Singla, M.; Jaggi, N. Enhanced Hydrogen Sensing Properties in Copper Decorated Nitrogen Doped Defective Graphene Nanoribbons: DFT Study. *Phys. E Low-Dimens. Syst. Nanostruct.* **2021**, *131*, 114756. [[CrossRef](#)]
151. Ni, J.; Quintana, M.; Song, S. Adsorption of Small Gas Molecules on Transition Metal (Fe, Ni and Co, Cu) Doped Graphene: A Systematic DFT Study. *Phys. E Low-Dimens. Syst. Nanostruct.* **2020**, *116*, 113768. [[CrossRef](#)]
152. Zitoune, H.; Adessi, C.; Benchallal, L.; Samah, M. Quantum Transport Properties of Gas Molecules Adsorbed on Fe Doped Armchair Graphene Nanoribbons: A First Principle Study. *J. Phys. Chem. Solids* **2021**, *153*, 109996. [[CrossRef](#)]
153. Kuang, A.; Mo, M.; Kuang, M.; Wang, B.; Tian, C.; Yuan, H.; Wang, G.; Chen, H. The Comparative Study of XO<sub>2</sub> (X = C, N, S) Gases Adsorption and Dissociation on Pristine and Defective Graphene Supported Pt13. *Mater. Chem. Phys.* **2020**, *247*, 122712. [[CrossRef](#)]
154. Yang, L.; Xiao, W.; Wang, J.; Li, X.; Wang, L. Formaldehyde Gas Sensing Properties of Transition Metal-Doped Graphene: A First-Principles Study. *J. Mater. Sci.* **2021**, *56*, 12256–12269. [[CrossRef](#)]
155. Cai, Y.; Luo, X. First-Principles Investigation of Carbon Dioxide Adsorption on MN<sub>4</sub> Doped Graphene. *AIP Adv.* **2020**, *10*, 125013. [[CrossRef](#)]
156. Guo, J.; Liu, Z.; Liu, S.; Zhao, X.; Huang, K. High-Capacity Hydrogen Storage Medium: Ti Doped Fullerene. *Appl. Phys. Lett.* **2011**, *98*, 023107. [[CrossRef](#)]
157. Germán, E.; Alonso, J.A.; Janssens, E.; López, M.J. C<sub>60</sub>Co<sub>n</sub> Complexes as Hydrogen Adsorbing Materials. *Int. J. Hydrog. Energy* **2021**, *46*, 20594–20606. [[CrossRef](#)]
158. Arshadi, S.; Anisheh, F. Theoretical Study of Cr and Co- Porphyrin-Induced C<sub>70</sub> Fullerene: A Request for a Novel Sensor of Sulfur and Nitrogen Dioxide. *J. Sulfur Chem.* **2017**, *38*, 357–371. [[CrossRef](#)]
159. Chen, X.; Zhang, H.; Lai, N. Endohedral Metallofullerenes Mn@C<sub>60</sub> (M = Mn, Co, Ni, Cu; n = 2–5) as Electrocatalysts for Oxygen Reduction Reaction: A First-Principles Study. *J. Mater. Sci.* **2020**, *55*, 11382–11390. [[CrossRef](#)]
160. Zou, L.; Zhu, Y.; Cen, W.; Jiang, X.; Chu, W. N-Doping in Graphdiyne on Embedding of Metals and Its Effect in Catalysis. *Appl. Surf. Sci.* **2021**, *557*, 149815. [[CrossRef](#)]
161. Panigrahi, P.; Dhinakaran, A.K.; Naqvi, S.R.; Gollu, S.R.; Ahuja, R.; Hussain, T. Light Metal Decorated Graphdiyne Nanosheets for Reversible Hydrogen Storage. *Nanotechnology* **2018**, *29*, 355401. [[CrossRef](#)]
162. Yu, H.; Hui, L.; Xue, Y.; Liu, Y.; Fang, Y.; Xing, C.; Zhang, C.; Zhang, D.; Chen, X.; Du, Y.; et al. 2D Graphdiyne Loading Ruthenium Atoms for High Efficiency Water Splitting. *Nano Energy* **2020**, *72*, 104667. [[CrossRef](#)]
163. Zhai, X.; Yan, H.; Ge, G.; Yang, J.; Chen, F.; Liu, X.; Yang, D.; Li, L.; Zhang, J. The Single-Mo-Atom-Embedded-Graphdiyne Monolayer with Ultra-Low Onset Potential as High Efficient Electrocatalyst for N<sub>2</sub> Reduction Reaction. *Appl. Surf. Sci.* **2020**, *506*, 144941. [[CrossRef](#)]
164. Jasin Arachchige, L.; Xu, Y.; Dai, Z.; Zhang, X.L.; Wang, F.; Sun, C. Double Transition Metal Atoms Anchored on Graphdiyne as Promising Catalyst for Electrochemical Nitrogen Reduction Reaction. *J. Mater. Sci. Technol.* **2021**, *77*, 244–251. [[CrossRef](#)]
165. Chen, X.; Gao, P.; Guo, L.; Wen, Y.; Fang, D.; Gong, B.; Zhang, Y.; Zhang, S. High-Efficient Physical Adsorption and Detection of Formaldehyde Using Sc- and Ti-Decorated Graphdiyne. *Phys. Lett. A* **2017**, *381*, 879–885. [[CrossRef](#)]

166. Liu, J.; Wang, L.; Shen, X.; Gao, X.; Chen, Y.; Liu, H.; Liu, Y.; Yin, D.; Liu, Y.; Xu, W.; et al. Graphdiyne-Templated Palladium-Nanoparticle Assembly as a Robust Oxygen Generator to Attenuate Tumor Hypoxia. *Nano Today* **2020**, *34*, 100907. [[CrossRef](#)]
167. He, T.; Zhang, L.; Kour, G.; Du, A. Electrochemical Reduction of Carbon Dioxide on Precise Number of Fe Atoms Anchored Graphdiyne. *J. CO<sub>2</sub> Util.* **2020**, *37*, 272–277. [[CrossRef](#)]
168. Liu, X.; Tang, W.; Liu, S.; Chen, X.; Li, Y.; Hu, X.; Qiao, L.; Zeng, Y. CO Oxidation on Ni and Cu Embedded Graphdiyne as Efficient Noble Metal-Free Catalysts: A First-Principles Density-Functional Theory Investigation. *Appl. Surf. Sci.* **2021**, *539*, 148287. [[CrossRef](#)]
169. Vijay, D.; Sakurai, H.; Subramanian, V.; Sastry, G.N. Where to Bind in Buckybowls? The Dilemma of a Metal Ion. *Phys. Chem. Chem. Phys.* **2012**, *14*, 3057. [[CrossRef](#)] [[PubMed](#)]
170. Zhang, C.; Li, J.; Shi, C.; He, C.; Liu, E.; Zhao, N. Effect of Ni, Fe and Fe-Ni Alloy Catalysts on the Synthesis of Metal Contained Carbon Nano-Onions and Studies of Their Electrochemical Hydrogen Storage Properties. *J. Energy Chem.* **2014**, *23*, 324–330. [[CrossRef](#)]
171. Canales, M.; Ramírez-de-Arellano, J.M.; Magana, L.F. Interaction of a Ti-Doped Semi-Fullerene (TiC<sub>30</sub>) with Molecules of CO and CO<sub>2</sub>. *J. Mol. Model.* **2016**, *22*, 223. [[CrossRef](#)]
172. Canales-Lizaola, M.; Arellano, J.S.; Magaña, L.F. Hydrogen Molecule Adsorption on a Ti-Doped Graphene+ Semi-Fullerene Surface. *J. Phys. Conf. Ser.* **2019**, *1221*, 012081. [[CrossRef](#)]